Spindle rotation in human cells is reliant on MARK2-mediated equatorial spindle centering mechanism

Ihsan Zulkipli[2, 4*], Joanna Clark[2*], Madeleine Hart[1*], Roshan Shrestha[2, 5*], Parveen Gul[1], David Dang[1, 3], Tami Kasichiwin[1], Izabela Kujawiak[2], Nishanth Sastry[3] and Viji M. Draviam#[1, 2]

[*]Equal contribution authors

#Correspondence to v.draviam@qmul.ac.uk

[1]School of Biological and Chemical Sciences, Queen Mary University of London, London UK

[2]Department of Genetics, University of Cambridge, Cambridge, UK

[3]Department of Informatics, Kings College, London, UK

Current addresses:

[4]Pengiran Anak Puteri Rashidah Sa'adatul Bolkiah Institute of Health Sciences, Universiti Brunei Darussalam, Jalan Tungku Link BE1410, Brunei Darussalam

[5]Center for Cancer Research, National Cancer Institute, National Institutes of Health, Bethesda, MD 20892

Address correspondence to:

Viji M Draviam

School of Biological and Chemical Sciences

Queen Mary University of London

London E1 4NS

eTOC: Unlike man-made wheels that are centered and rotated via an axle, the mitotic spindle of a human cell is rotated by external cortical pulling mechanisms. The Draviam group identifies MARK2's role in equatorial spindle centering and astral microtubule length, which in turn control spindle rotation.

ABSTRACT

The plane of cell division is defined by the final position of the mitotic spindle. The spindle is pulled and rotated to the correct position by cortical Dynein. However, it is unclear how the spindle's rotational center is maintained and what the consequences of an equatorially off-centered spindle are in human cells. We analysed spindle movements in 100s of cells exposed to protein depletions or drug treatments, and uncover a novel role for MARK2 in maintaining the spindle at the cell's geometric center. Following MARK2 depletion, spindles glide along the cell-cortex leading to a failure in identifying the correct division-plane. Surprisingly, spindle off-centering in MARK2-depleted cells is not due to excessive-pull by Dynein. We show that MARK2 modulates mitotic microtubule growth and length and co-depleting MCAK, a microtubule destabilizer, rescues spindle off-centering in MARK2-depleted cells. Thus, we provide the first insight into a spindle centering mechanism needed for proper spindle rotation and in turn, the correct division-plane in human cells.

INTRODUCTION

Loss of tissue organisation is a hallmark of aggressive carcinomas. In epithelial tissues, during cell division, the position of the mitotic spindle defines the plane of division and in turn, the position of daughter cells within the growing and stratifying epithelial tissue (reviewed in (Chin et al., 2014), Macara et al., 2014, Kulukian and Fuchs., 2013). The spindle is brought to the correct position by cortical Dynein-mediated forces that pull and rotate the spindle – how these pulling forces are counteracted to maintain the spindle's center of rotation is an intriguing physical and biological problem. Spindle centering forces were recently measured in worm embryos (Garzon-Coral et al., 2016) that are 10 times larger than human cells. Master regulators that sense and control spindle centering are not known in human cells, although changes in microtubule dynamics can alter spindle centering (Draviam et al., 2006), suggesting the existence of a centering mechanism in human cells as well.

Unlike spindle centering mechanisms (in the XY plane), spindle orientation mechanisms (in the Z plane) have been explored in detail in human cells. Proper 3-dimensional orientation of the spindle requires the interactions of astral microtubules with cytoplasmic and cortical force generators (O'Connell and Wang, 2000; Wühr et al., 2010; Kimura and Kimura, 2011; Kiyomitsu and Cheeseman, 2012; Collins et al., 2012; Markus and Lee., 2011). In cell cultures, Dynein is required to rotate and orient the spindle along a predetermined axis: the interphase long-axis of the cell (O'Connell and Wang, 2000; Corrigan et al., 2013). Importantly, two pathways that influence cortical Dynein – the LGN-NuMA-Gαi pathway (Kotak et al., 2012) and CHICA dependent Dynein signaling pathway (Dunsch et al., 2012) – orient the spindle parallel to the substratum, and excessive Dynein activity can cause spindle tumbling with respect to the substratum (Samora et al., 2011; Kotak et al., 2012). Thus, cortical Dynein-mediated pull is currently considered to be the primary force-generating pathway for powering spindle movements in human cells. In contrast, in the yeast *S.cerevisiae*, Dynein is dispensable for early spindle rotation or alignment and is essential only for the later translocation of the spindle into the bud-neck (Sheeman et al., 2003; Huisman and Segal, 2005; Hoopen et al., 2012). Whether similar mechanisms independent of cortical Dynein operate in human cells to dynamically control spindle positions is not known.

MARK2$^{Par1b/EMK1}$ (hereafter referred as MARK2) of the MARK family of kinases is evolutionarily conserved from yeasts to humans. MARK2 null mice are dwarf, with most tissues proportionately smaller, hypofertile, lean and resistant to high-fat diet induced weight gain (Bessone et al., 1999; McDonald., 2007). In nematodes, mutations in par-1 disrupt spindle positioning leading to disorganized embryos that lack germ cells (Guo and Kemphues, 1995). In flies, mutations in par-1 disrupt the oocyte microtubule network leading to defects in posterior patterning of the embryo (Shulman et al., 2000). In mouse hepatocytes, MARK2 is required for the asymmetric inheritance of apical domains through cell division (Slim et al., 2013). However, the precise role of MARK2 during the process of spindle orientation in human cells is not clear.

MARK2's role in the regulation of interphase microtubule dynamics have been characterized in several cell lines (Cohen et al., 2004; Nishimura et al., 2012; Mandelkow, 2004; Hayashi et al., 2011; Schaar et al., 2004; Sato et al., 2013; Sato et al., 2014). Whether MARK2 controls mitotic microtubule dynamics is not known.

To study spindle rotation and centering mechanisms, we used time-lapse microscopy to track changes in spindle positions in 100s of dividing human epithelial cells. We employed our quantitative single-cell methodology to link a variety of interphase cell shapes to dynamically changing spindle positions in cultures that retain cell-cell contacts (Corrigan et al., 2013), so that we can systematically compare the roles of proteins in centering, rotating and oscillating movements of the mitotic spindle. We report that the spindles of MARK2-depleted cells are equatorially off-centered and the spindles undergo gliding instead of rotational movements. In the absence of MARK2, even spindles born close to the geometric center of the cell undergo dramatic off-centering and remain equatorially off-centered until anaphase. Importantly, equatorially off-centered spindles of MARK2-depleted cells fail to rotate properly towards the correct final position, pre-determined by interphase cell shape. This shows the importance of equatorial centering mechanisms in controlling spindle rotation and also, determining the correct division-plane. To identify the underlying molecular cause for off-centered spindles in MARK2-depleted cells, we studied the behaviour of cortical Dynein and astral microtubules. MARK2-depleted cells display longer astral microtubules, increased mitotic microtubule growth rates, and diffuse cortical Dynein along the cell cortex. Equatorial off-centering in MARK2-depleted cells could not be simply explained by excessive pulling by cortical Dynein because

the co-depletion of LGN leads to loss of cortical Dynein and spindle rotation, as expected, but spindles remain equatorially off-centered. In contrast, disrupting microtubule dynamics through MCAK depletion rescues the spindle off-centering phenotype in MARK2-depleted cells. We propose a model where cortical Dynein mediated pulling forces are actively counteracted by MARK2-mediated spindle centering mechanism to ensure the successful rotation of the spindle towards its pre-determined final position. Thus, this study uncovers the role and regulation of equatorial spindle centering in determining the correct plane of division in human cells.

RESULTS

Equatorial centering of the spindle is an early mitotic event

Using our single-cell method developed to track the spindle's biased rotation to its final position using interphase cell shape (Corrigan et al., 2013; 2015), we studied mitotic spindle movements from Nuclear Envelope Breakdown (NEBD) to anaphase onset in epithelial cell cultures that retained cell-cell and cell-substrate contacts. To study the range of spindle centering and off-centering events, we tracked spindle movements, once every four minutes, in a spindle reporter cell line HeLa$^{\text{His2B-GFP; mCherry-Tubulin}}$ that constitutively expresses low levels of mCherry-Tubulin and Histone2B-GFP(Corrigan et al., 2013). We assessed the extent of spindle centering along two axes: (i) the equatorial axis, by measuring the nearest distance between spindle equator and the cortex (for equatorial centering) and (ii) the pole-to-pole axis, by measuring the nearest distance between the spindle pole and cortex (for longitudinal centering) (Fig 1a). Analysis of mCherry-Tubulin signals in time-lapse movies showed that at the time of mitosis onset (marked by NEBD), spindles born in the geometric center are retained in the center, while spindles born away from the geometric center are actively brought to the centre within the first 12 minutes of NEBD (Fig 1a and 1b). We observed that equatorial spindle centering did not require a mature spindle structure, as equatorial centering was observed even in immature and bent spindles (compare Fig 1b and 1c). In contrast, and as reported earlier (Kiyomitsu and Cheeseman, 2012; Corrigan et al., 2013; Kotak et al., 2012), centering along the spindle's longitudinal pole-to-pole axis was dislodged by spindle oscillations (Fig 1a). Consequently, longitudinal off-centering of spindles arise as part of the normal

spindle oscillatory movement in late metaphase (Fig 1a). We conclude that the equatorial centering of the spindle apparatus is accomplished very early on during mitosis.

Equatorial centering of spindles fail in the absence of MARK2

To identify the molecular players required for the equatorial centering of the mitotic spindle, we used time-lapse microscopy and followed spindle movements in HeLa$^{\text{His2B-GFP; mCherry-Tubulin}}$ cells depleted of LGN, MARK2$^{\text{Par1b}}$ or PAR3, using multiple siRNA oligos. To confirm the extent of protein depletion in the cells studied using time-lapse microscopy, we collected cell lysates after each time-lapse imaging session (Fig 1d). Fluorescent immunoblots of lysates showed that greater than 90% of protein depletion was achieved following respective siRNA treatments (Fig 1f, g and 1h**).**

Analysis of time-lapse movies of HeLa$^{\text{His2B-GFP; mCherry-Tubulin}}$ cells showed normal equatorial centering of the spindle in cells depleted of LGN or PAR3 (Fig 1e, 1i and 1j**)**. In contrast, equatorial centering of spindles was severely disrupted in MARK2-depleted cells, compared to Control or LGN or PAR3 depleted cells (Fig 1e, 1i-1k**)**, revealing MARK2 as the first kinase with a role in the equatorial centering of the human mitotic spindle.

MARK2$^{\text{Par1b}}$ but not MARK3 $^{\text{Par1c}}$ is required for equatorial spindle centering

To confirm that MARK2 siRNA induced spindle centering defects are specific to MARK2 depletion and not an off-target effect we used two strategies: first, we confirmed that two different siRNA oligos against MARK2 caused the spindle off-centering defect. Time-lapse movies of HeLa$^{\text{His2B-GFP; mCherry-Tubulin}}$ cells showed equatorially off-centered mitotic spindles following the treatment with either MARK2-1 or MARK2-2 siRNA, but not control siRNA (Fig 2a and Supplementary Figure 1a). Quantitative analysis showed that 12 minutes after NEBD, equatorially centered spindles were found only in 28% and 38% of MARK2-1 and MARK2-2 siRNA treated cells, respectively, compared to 90% of control siRNA treated cells (Fig 2b). The severity of the spindle off-centering phenotype (Supplementary Figure 1a and Fig 2a) correlated well with the extent of MARK2 depletion (Fig 1h). Thus, two different siRNA-mediated depletions of MARK2 perturb the equatorial centering of mitotic spindles.

As a second strategy, to fully confirm that the equatorial centering defect observed in MARK2-siRNA treated cells is specifically due to MARK2 depletion and not an artifact due to off-target depletion, we generated siRNA resistant form of human MARK2 fused to YFP (hMARK2 ^{siRes} -YFP) and expressed it in low levels using a Tet-inducible system (Fig 2c). Following MARK2 siRNA treatment, hMARK2^{siRes}-YFP expressing cells (green cells) showed normally centered metaphase chromosomes, whereas, non-green cells showed equatorially off-centered chromosome positions (Fig 2d and Supplementary Figure 1b). Thus, MARK2 depletion induced spindle centering can be rescued by Tet-inducible expression of human MARK2 ^{siRes}-YFP. We conclude that MARK2 is required for the equatorial centering of mitotic spindle.

Furthermore, in cells treated with two different siRNA against MARK3^{Par1c}, a close family member of MARK2, we observed normal equatorial centering of spindles, similar to control siRNA treated cells (Supplementary Figure 1c and 1d). We conclude that MARK2, but not its close relative MARK3, is required for equatorial centering of the spindle.

Equatorial spindle centering is regulated differently in early and late mitosis

Biased rotation of the spindle occurs in early mitosis (Corrigan et al., 2013). We were intrigued to find that equatorially off-centered spindles of MARK2-depleted cells were observed primarily in early mitosis and these off-centered spindles were frequently restored back to the center in anaphase (Supplementary Figure 1a). To confirm this, we quantitatively compared early and late mitotic spindle positions in MARK2-depleted cells and found that spindles were equatorially centered normally in anaphase but not early mitosis (Fig 2e). We conclude that at least two equatorial spindle-centering mechanisms operate in human cells, which are mitotic phase dependent. MARK2 is required for spindle centering in early mitosis when the spindle undergoes rotation.

Equatorial centering is required for proper spindle rotation, oscillation and biased division-plane

The plane of epithelial cell division is pre-determined by interphase cell shape and cell-cell or cell-substrate contact sites (reviewed in (Chin et al., 2014)). We reported previously that the mitotic spindle first rotates with a directional bias towards the

interphase cell's long axis (during prometaphase when chromosomes congress) and then remains oriented along the long axis where it undergoes spindle oscillations (until anaphase when chromosomes segregate)(Corrigan et al., 2013;Corrigan et al., 2015). Whether any of these key mitotic events are perturbed in cells that fail to equatorially center their spindles is not known. Hence, we studied if MARK2-depleted cells displayed normal chromosome congression, chromosome segregation, spindle rotation, spindle oscillation and spindle orientation along the long-axis of the cell. Time-lapse movies of HeLa$^{His2B\text{-}GFP;\ mCherry\text{-}Tubulin}$ cells treated with MARK2 siRNA showed no significant difference in chromosome congression and segregation times, compared to control cells (Supplementary Figure 2a-d). However, the analysis of spindle movements indicated a striking reduction in spindle rotation or oscillatory pole-to-pole movements in MARK2-depleted cells compared to controls (Fig 2a, 3a and 3b; Supplementary Movies 1-3). Importantly, despite the absence of pole-to-pole oscillations, spindles in MARK2-depleted cells were dynamic and displayed gliding movements along the cell cortex (Fig 2a, 3a and 3b). Unlike the equatorially centered spindles in control cells that displayed biased rotation towards the interphase long-axis (4min to 12min; Fig 3a), the off-centered spindles in MARK2-depleted cells showed a prolonged duration of gliding motion along the cell cortex; thus, the absence of spindle centering disrupted normal spindle rotation. The gliding motion and lack of rotation was most obvious in MARK2-depleted cells when congression was occasionally delayed (Supplementary Movie 3). In summary, MARK2 depletion disrupts equatorial spindle centering, spindle rotation and oscillations (Fig 3b) – events that precede anaphase.

Because spindle centering, rotation and oscillations were all disrupted in MARK2-depleted cells, we tested whether spindles could define the plane of cell division normally. To determine the efficiency with which cells could properly rotate their spindles and arrive at the final predefined position along the interphase long-axis, we performed semi-automated analysis of our movies using our *Spindle3D* software (Corrigan et al., 2013). Analysis of final spindle orientation angles at the metaphase-anaphase transition showed a statistically significant reduction in the percentage of cells that correctly aligned the spindle along the interphase long-axis following MARK2 depletion, compared to control depletion (Fig 3c and 3d). Thus, MARK2 depletion induced spindle off-centering is coincident with severe defects in both spindle rotation and identifying the correct plane of cell division (Fig 3d).

MARK2 depletion delays but does not abrogate mitotic cell rounding

Compared to Control depleted cells, MARK2-depleted cells showed a delay in mitotic cell rounding (Supplementary Figure 2e). However, mitotic cell rounding was not completely abrogated, as the vast majority of MARK2-depleted cells had completed mitotic-rounding in late prometaphase (at least 8 minutes prior to anaphase onset; Supplementary Figure 2e). In contrast, equatorial spindle centering remained severely compromised in late prometaphase MARK2-depleted cells (Supplementary Figure 2f); at this stage spindles were bipolar and normally oriented parallel to the substratum as assessed by spindle-pole positions (Supplementary Figure 2g). Based on these analyses, we conclude that equatorial spindle off-centering in MARK2-depleted cells is not directly caused by the delay in mitotic cell rounding.

MARK2 localises to centrosomes and cell cortex and its depletion alters mitotic microtubule growth and function

To understand the underlying reason for spindle off-centering in MARK2-depleted cells, we next studied the localization of MARK2 in HeLa cells using YFP-tagged MARK2. YFP-MARK2 localised to both interphase and mitotic centrosomes independent of microtubules (Supplementary Figure 3). In mitotic cells, MARK2 distinctly localised to the cell cortex and faintly associated with the mitotic spindle in a microtubule-dependent manner (Supplementary Figure 3b and 3d).

We next investigated if depletion of MARK2 altered the distribution of astral microtubules in mitosis. Following a brief exposure to ice-cold methanol for 60 seconds, we immunostained siRNA treated cells using tubulin antibodies to assess the status of cold stable astral microtubules (Supplementary Figure 4a). Compared to Control siRNA treated cells, MARK2 siRNA depleted cells showed a noticeable increase in astral microtubule length and density near poles (Fig 4a and Supplementary Fig 4b). Mean lengths of cold-stable astral microtubules were 1.69 (SD = 0.61) μm (n = 6 cells) following control siRNA treatment and 3.27 (SD = 1.25) μm (n = 10 cells) following MARK2 siRNA treatment. Mean densities of cold-stable astral microtubules near spindle pole area were ~2 MTs/23μ^2 (n = 10cells) following Control siRNA treatment and ~6 MTs/23μ^2 (n = 10cells) following MARK2 siRNA treatment. These findings in mitotic cells are consistent with the reported interphase

role of MARK2 as an enhancer of microtubule destabilisation, by controlling microtubule lifetime and growth rate (Nishimura et al., 2012).

Whether MARK2 regulates mitotic microtubule dynamics is not known. To address this, we depleted MARK2 in cells expressing EB3-TdTomato (HeLa EB3-TdTomato), a routine marker for growing mitotic microtubule-ends (Tamura et al., 2015; Nakai et al., 2015; Shrestha et al., 2014; Iorio et al., 2015), and measured instantaneous velocity of growing microtubules in the metaphase spindle. We found a small but significant increase in mitotic microtubule growth rates in MARK2-depleted cells compared to control depleted cells (Fig 4b). Due to the modest changes in microtubule growth rates following MARK2 depletion, we used a sensitive mitotic microtubule function assay to confirm the role of MARK2 in regulating mitotic microtubules. We treated cells with Nocodazole to fully disassemble mitotic spindle microtubules and then washed off the drug to study the rate of spindle reassembly, which is dependent on microtubule function. As a positive control, Nocodazole washed off cells were exposed to 2ME2 (2-methyl Estradiol), a microtubule pausing drug (Corrigan et al., 2013) that is expected to delay bipolar spindle reassembly. To study bipolar spindle reassembly efficiency in the presence and absence of MARK2, we fixed and immunostained cells at various time-points after Nocodazole wash-off. As expected, 10 minutes following Nocodazole wash-off, control cells form multipolar spindles that rapidly coalesce into a single bipolar spindle (Tulu et al., 2006). In contrast, MARK2 siRNA or 2ME2 treated cells were delayed in coalescing multipolar spindles into bipolar ones, compared to control siRNA treated cells (Fig 4c), providing further evidence for the role of MARK2 in regulating mitotic microtubule function. We conclude that MARK2 kinase controls microtubule plus-end growth rates, astral microtubule length and microtubule function during mitosis.

Cortical Dynein is diffuse but spindle movement rates are unperturbed in MARK2-depleted cells

Cortical Dynein is required for a stable 3-dimensional positioning of the spindle parallel to the substratum and also for spindle oscillations along the longitudinal pole-to-pole axis (Kotak et al., 2012; Kiyomitsu and Cheeseman, 2012; Corrigan et al., 2013). So, we tested whether cortical Dynein localization is perturbed following MARK2 depletion using a HeLa$^{DHC1\text{-}GFP}$ cell line expressing GFP-fused to mouse

Dynein Heavy Chain 1 (DHC1) under the control of its endogenous promoter(Poser et al., 2008).

Using DHC1-GFP localization at spindle poles, we once again confirmed equatorially off-centered spindles in HeLa$^{DHC1\text{-}GFP}$ cells treated with MARK2 siRNA (Fig 5a). As expected(Kiyomitsu and Cheeseman, 2012)(Tame et al., 2014), in Control siRNA treated cells DHC1-GFP signal at the cortex was asymmetrically enriched in a small region (marked by blue arrowhead in Fig 5a; referred as 'crescent' in Fig 5b) and was mostly excluded in regions proximal to the spindle pole (Fig 5a). However, in MARK2 siRNA treated cells DHC1-GFP signal at the cortex was distributed along a wider region compared to controls and lacked the crescent-like enrichment (marked by green arrowhead in Fig 5a; referred as 'diffuse' in Fig 5b), although DHC1-GFP was normally excluded at the cell cortex proximal to the spindle pole (Fig 5a). This normal exclusion of DHC1-GFP signal from cortical areas close to the spindle pole and chromosomes suggest that Plk1 and Ran dependent mechanisms that exclude DHC-GFP from the cortex(Kiyomitsu and Cheeseman, 2012) are unlikely to be perturbed following MARK2 depletion (Fig 5a). Because chromosome and spindle pole positions can influence the position of cortical Dynein localization (Kiyomitsu and Cheeseman, 2012), the diffuse cortical Dynein localization could be a consequence of off-centered spindles in MARK2-depleted cells.

To test whether the diffuse cortical localization of Dynein can impair the extent of spindle movement, we measured spindle displacement towards the cortex in Control and MARK2-depleted HeLa$^{DHC1\text{-}GFP}$ cells using DHC-GFP as a spindle pole marker. Comparing the distribution of spindle pole displacement between Control and MARK2-depleted cells showed no significant difference (Fig 5c). Thus, despite the equatorial off-centering of spindles and diffuse localization of cortical Dynein, spindle displacement extent *per se* is not noticeably impaired in MARK2-depleted cells, suggestive of comparable pulling towards the cortex in the presence and absence of MARK2.

Spindle off-centering in MARK2-depleted cells is not due to excessive pulling by cortical Dynein

Longer astral microtubules in MARK2-depleted cells compared to Control cells (Fig 4a) raised the possibility that spindle off-centering may arise from prolonged pulling of microtubules by cortical Dynein, which may have been missed in our spindle

displacement studies. Therefore, we co-depleted LGN (cortical Dynein platform) and MARK2 and used time-lapse microscopy to assess equatorial centering of spindles in the absence of cortical Dynein. We first confirmed that cortical Dynein is absent in LGN and MARK2 co-depleted HeLa$^{DHC1\text{-}GFP}$ cells (Fig 6d).

As expected from a loss of cortical Dynein phenotype, the spindles of LGN and MARK2 co-depleted cells did not display much movement throughout mitosis (Fig 6a). Importantly, comparing the extent of spindle centering in LGN *versus* LGN and MARK2 co-depleted HeLa cells$^{His2B\text{-}GFP;\ mCherry\text{-}Tubulin}$ showed increased spindle off-centering in co-depleted cells (Fig 6a-6c), confirming MARK2's role in spindle centering. Because LGN depletion did not fully rescue the equatorial centering defect seen following MARK2 depletion (Fig 6a-6c), we conclude that spindle off-centering in MARK2-depleted cells is not simply due to excessive pull by cortical Dynein.

Importantly, those spindles born at the geometric center remained centered in MARK2 and LGN co-depleted cells, unlike MARK2 alone depleted cells where spindles born at the geometric center become actively off-centered (Compare Fig 6a and 2a). These data suggest that MARK2 activity plays an important unrecognised role in resisting an outwardly pull of the spindle by cortical-Dynein in specifically in early mitosis.

In summary, the persistence of off-centered spindles in cells co-depleted of LGN and MARK2 demonstrate a role for MARK2 in equatorial centering of spindles independent of the LGN pathway. We conclude that equatorial off-centering of spindles in MARK2-depleted cells is not due to excessive pull by cortical Dynein.

MARK2 loss induced spindle off-centering can be rescued by MCAK depletion

MARK2 depletion induced an increase in microtubule plus-end growth rate. So, we tested if reducing plus-end dynamics could rescue MARK2 depletion induced spindle off-centering. For this purpose, we chose to deplete MCAK, a microtubule destabilizer, that tracks with microtubule tips during mitosis (Domnitz et al., 2012). MCAK depletion causes an increase in astral microtubule stability (Rizk et al., 2009) and reduction in microtubule growth velocities (Braun et al., 2014). We had previously shown that MCAK is not required for spindle orientation success or rotational bias of spindles (Corrigan et al., 2013), but whether it is important for equatorial centering of the spindle was not known. We first analysed spindle centering success following MCAK depletion in HeLa$^{His2B\text{-}GFP;\ mCherry\text{-}Tubulin}$ cells. We observed

no significant difference in equatorial spindle centering extent between MCAK *versus* Control depleted cells (Compare Fig 7b and 'control' in Fig 2a), although as reported (Kline-Smith et al., 2004) chromosome congression time was prolonged and lagging chromosomes were seen in MCAK depleted cells (Average NEBD to anaphase onset time: Control siRNA: 30 min (n=66 cells); MCAK siRNA: 41 min (n=117 cells)). We conclude MCAK is dispensable for the equatorial centering of mitotic spindles.

To test if MCAK depletion could rescue MARK2 depletion induced off-centering of spindles, we analysed spindle positions in time-lapse movies of cells co-depleted of MCAK and MARK2. The percentage of cells with equatorially centered spindles at 8 min and 12 min following NEBD was significantly increased following the co-depletion of MCAK and MARK2, compared to MARK2 depletion alone, indicating a rescue of the spindle off-centering phenotype induced by MARK2 depletion (Fig 7a-d).

Although the spindle off-centering phenotype was rescued, mitotic cell rounding delay remained until late prometaphase in cells co-depleted of MARK2 and MCAK (Supplementary Fig 4f). These findings show that the depletion of MCAK specifically rescues the spindle centering defect but not the mitotic cell rounding delay in MARK2-depleted cells.

We investigated if MCAK depletion rescued spindle off-centering in MARK2-depleted cells simply by further increasing the length of astral microtubules. For this purpose, we briefly exposed cells to cold and immunostained siRNA treated cells using tubulin antibodies to assess the status of cold stable astral microtubules (Supplementary Fig 4a). Analysing the length of astral microtubules relative to pole-cortex distance in centered and off-centered spindles showed a comparable increase in astral microtubule occupancy in cells depleted of MARK2, MCAK or both, compared to controls (Supplementary Fig 4b-d). These findings show that the rescue of spindle centering is not simply due to a dramatic increase in the lengths or densities of astral microtubules in MCAK and MARK2 co-depleted cells. Moreover, using immunostaining, we did not observe any obvious change in colocalization between MCAK and EB3 (a microtubule plus-end marker) following MARK2 depletion (Supplementary Fig 4e), ruling out a direct role for MARK2 in altering MCAK localization or function.

Detailed analysis of spindle positions once every four minutes following NEBD (Fig 7d) showed that the rescue of spindle centering is dynamic: in conditions

where MCAK alone or both MCAK and MARK2 were depleted, off-centered spindles were rapidly restored back to the center unlike in MARK2-depleted cells. These data show that MARK2 depletion induced equatorial off-centering of spindles is being dynamically rescued by co-depleting the microtubule depolymeriser, MCAK. Importantly, MCAK co-depletion rescued the diffuse cortical Dynein localization observed in MARK2 depleted cells (Fig 7e and 7f), showing that cortical Dynein crescents are reliant on equatorial spindle centering status. We conclude MARK2 depletion induced equatorial spindle off-centering is dynamically rescued by MCAK depletion, highlighting the importance of MARK2-mediated modulation of microtubule dynamics in the equatorial centering of spindles.

DISCUSSION

By tracking the temporal evolution of spindle positions, we demonstrate that proper rotation of the mitotic spindle requires two closely related mechanisms: MARK2-mediated spindle centering and cortical Dynein-mediated spindle pulling. While Dynein-mediated pull powers the movement of spindles, we show that MARK2 is needed to restore an off-centered spindle back to the center of the cell: a loss of either of these pathways will disrupt spindle rotation leading to an incorrect division-plane. By showing that MARK2's centering role is dependent on microtubule dynamics, our findings reveal a previously unrecognized spindle centering mechanism that is crucial for successful spindle rotation. We present a dynamic model wherein the rotation of mitotic spindle to a pre-determined position is dependent on both cortical Dynein mediated spindle movement and MARK2 mediated spindle centering mechanisms.

In vitro studies of microtubule asters, devoid of rotation, show that although Dynein can support centration it is not needed for centering the asters(Laan et al., 2012). In worm embryos, cortical force generation in fact antagonizes metaphase spindle centration (Garzon-Coral et al., 2016). In agreement, our *in vivo* studies of LGN-depleted cells show that cortical Dynein is dispensable for spindle centering, in metaphase, along both the equatorial and longitudinal axes. Therefore, cortical Dynein is not required for equatorial spindle centering in human cells, but is instead required for dislodging the spindle from its position, as part of the spindle rotation process (Fig 7g). Thus, by using MARK2 depletion as a molecular probe we have

uncovered an essential role for equatorial spindle centering in forming cortical Dynein crescents and in turn, mediating proper spindle rotation.

We find that cold-stable astral microtubule length and density are increased in MARK2-depleted cells, similarly to cells depleted of MCAK, a potent MT destabilizer (reviewed in (Tamura and Draviam, 2012)) revealing MARK2's significant role in regulating astral microtubules. During interphase, MARK2 regulates the levels of MAP2 and Tau proteins on the microtubule (Drewes et al., 1995; Illenberger et al., 1996; Drewes et al., 1997), whereas the c-terminus of MCAK by itself regulates its binding to the ends of microtubules (Talapatra et al., 2015). Consistent with this difference in regulation, we find that MARK2 depletion increases microtubule growth speed, whereas MCAK depletion reduces microtubule growth velocities(Braun et al., 2014). These two microtubule regulatory pathways are likely to crosstalk as the co-depletion of MCAK dynamically rescues both the off-centered spindles and loss of cortical Dynein crescents in MARK2-depleted cells.

We hypothesize that microtubule-ends are sufficient, given certain physical constraints, to drive cell shape associated spindle centering in human cells. A similar conclusion has been drawn for nuclear centering (Zhao et al., 2012) and centrosome centering in interphase cells (Zhu et al., 2010) and spindle centering in worm embryos (Garzon-Coral et al., 2016). In this context our discovery of MARK2's role in controlling mitotic microtubule dynamics is important. The MARK family of kinases were originally identified in a screen for kinases that phosphorylate microtubule-associated proteins (Tau, MAP2 and MAP4) and trigger microtubule disruption in interphase (Drewes et al., 1995; Illenberger et al., 1996; Drewes et al., 1997). Subsequently, MARK mediated regulation of microtubule dynamics during interphase were characterized in several cell lines (Cohen et al., 2004; Nishimura et al., 2012; Mandelkow et al., 2004; Hayashi et al., 2011; Schaar et al., 2004). Our findings extend this interphase role of MARK2 to mitosis for the first time. Previously it was not known if the MARK family played any role in dividing human epithelial cells, whether through its regulation of microtubule dynamics or otherwise.

Finally, we provide the first evidence for a cell cycle dependent role for MARK2 in spindle centering, during early mitosis when spindle rotation occurs. Several microtubule associated proteins, EB1 and APC, actin meshwork regulators, Myosin-X, Abl1, PI(3)K, PAK2 and LIMK1, β□-integrin and Cdc42 (Kotak et al.,

2012; Kiyomitsu and Cheeseman, 2012; Matsumura et al., 2012; Mitsushima et al., 2009; Toyoshima et al., 2007; Samora et al., 2011; Draviam et al., 2006; Dunsch et al., 2012; Toyoshima and Nishida, 2007; Kaji et al., 2008) are known to be important for spindle orientation, but it is not clear if these are mitotic phase specific roles. Even for previously reported spindle centering regulators - Moesin, LIMK1 and the microtubule-end binding proteins EB1 and APC (Draviam et al., 2006; Roubinet et al., 2011; Kunda et al., 2008; Carreno et al., 2008; Kaji et al., 2008) – it is not clear if disrupting their role leads to spindle gliding instead of spindle rotation in a cell cycle regulated manner. However, it is clear that proteins that occupy microtubule-ends are mitotic-phase dependent (Tamura et al., 2015; Syred et al., 2013). Our study shows that depletion of MARK2^{Par1b} alone, but not LGN, PAR3, MARK3^{Par1c} or MCAK, severely disrupts the equatorial centering in pre-anaphase spindles. In contrast, codepletion of LGN and MARK2 disrupts equatorial centering in anaphase spindles as well, showing the temporally separable roles of LGN and MARK2. How MARK2 regulates mitotic microtubule dynamics and restores spindle centering in a cell cycle specific manner are important questions for the future.

MARK2 loss does not perturb chromosome congression or segregation, despite impairing spindle centering and spindle rotation. This suggests that spindle-centering mechanisms are exquisitely sensitive to microtubule dynamics compared to other microtubule driven mitotic events. A wider and important biomedical implication of this study is that spindle positioning, and hence cell fate decisions and in turn tissue organization (Patel et al., 2016; Chin et al., 2014), might be more readily disrupted relative to chromosomal stability following anti-microtubule cancer therapies.

MATERIALS AND METHODS

Cell culture and synchronization

HeLa cells were cultured in Dulbecco's Modified Eagle's Media(Tergaonkar et al., 1997) supplemented with 10% FCS and antibiotics, Penicillin and Streptomycin, and plated onto glass-bottomed dishes (LabTek) or 13mm round coverslips for imaging. For inhibition studies, cells were treated with 10 μM MG132 (1748, TOCRIS). Cells were synchronised using a single aphidicolin (1μg/ml) block for 24 hours and then released for 7 hours prior to filming.

Cell line generation

HeLa$^{hMARK2\text{-}siRES\text{-}YFP}$ cell line was generated by transfecting a Tet-inducible expression vector encoding hMARK2-siRes-YFP and followed by colony picking. Cell line generation procedures were followed according to the FRT/TO system protocol (Invitrogen).

Plasmid and siRNA transfections

HeLa cells were transfected with siRNAs or plasmid vectors as described in(Shrestha et al., 2014). siRNA oligos used against MARK2 (CCUCCAGAAACUAUUCCGCGAAGUA; MARK2-1 and UCUUGGAUGCUGAUAUGAACAUCAA; MARK2-2), LGN(Corrigan et al., 2013), MARK3 (AUAUGUUGCGGUUCGCCGUUCCCGG; MARK3-2 and GCGGUAAACUCGACACGUU; MARK3-3) and PAR-3 (CAACAGCUGGCUUCCUCAAGCAGAA; PAR3-1 and GCAAGAGGCUUAAUAUCCGACUUAA; PAR3-2) were purchased from Dharmacon. Sequences of all plasmids are available upon request.

Live-cell time-lapse imaging and analysis

Cells were transfected with siRNA oligos or plasmid vectors, 48 or 24 h, respectively, prior to imaging and transferred to Leibovitz's L15 medium (Invitrogen) for imaging at 37°C. To observe chromosome and spindle movements, images were acquired with exposures of 0.1 s from at least 3 Z-planes, 3□μ□ apart, every 4 minutes for 5 h using

a 40 times NA 0.75 objective on an Applied Precision DeltaVision Core microscope equipped with a Cascade2 camera under EM mode. For imaging plus-end dynamics, images were acquired with exposures of 0.04 s from at least 10 Z-planes, 0.1□μ□ apart, every 10 seconds for 5 minutes using a 100 times NA 1.2 objective on the microscope described above. For imaging DHC-GFP signals, images were acquired with exposures of 0.04 s from at least 10 Z-planes, 0.1□μ□ apart, every 1 minute for 10 minutes using a 100 times NA 1.2 objective on the microscope described above. Time-lapse movies were analysed manually using Softworx^{TM}. Spindles in HeLa$^{His\text{-}GFP;mCherry\text{-}Tub}$ cells were visually scored as equatorially off-centered when unequal distances were observed between the cell cortex and the two opposing edges of metaphase plate (Histone-GFP signal) or the cell cortex and the two walls of the spindle at the equator (mCherry-Tubulin signal). In HeLa$^{DHC\text{-}GFP}$ cells, the pole-to-pole axis and spindle walls (DHC-GFP signal) were used to similarly assess spindle centering at the equator.

Immunoflourescence and immunoblotting

For immunofluorescence, antibodies against GFP (1:1000, Roche; 1181446001), MARK2 (1:500, Novus Biologicals; H00002011-M01), MARK3 (1:1000, Cell Signalling; 9311), PAR3 (1:1000, Millipore Corporation; 07-330), α-tubulin (1:500, Abcam, Ab6160), EB3 (Abcam), MCAK ((Andrews et al., 2004)) and β-tubulin (1:1000, Sigma; T4026) were used. Images of immunostained cells were acquired using 100 times NA 1.2 objective on a DeltaVision Core microscope equipped with CoolSnap HQ Camera (Photometrics). For immunoblotting, antibodies against γ-Tubulin (Sigma; T6793) and others indicated above were used. Immunoblots were developed using fluorescent secondary antibodies (LICOR) and fluorescent immunoblots were quantified using the Odyssey (LI-COR) software.

Nocodazole wash-off assay

Cells were exposed to 1.7 μM of Nocodazole (Fisher Scientific) for 3 hours to depolymerize microtubules. Nocodazole was removed by washing cells three times with warm PBS and cells were allowed to recover for 10 minutes in nocodazole-free Complete DMEM. Cells were fixed and immunostained using anti-Tubulin antibody.

Statistical Analysis

SD values are SEM values obtained across experiments, cells or kinetochores as indicated in legend. p-values representing significance were obtained using Mann-Whitney U test, Proportion test or Paired sample t-test.

Online Supplementary Material

Fig. S1 shows MARK2 but not MARK3 is required for equatorial spindle centering. Fig. S2 shows normal chromosome congression and segregation in MARK2 depleted cells. Fig S3 shows MARK2 localisation in interphase and mitosis. Fig S4 shows the rescue of MARK2-depletion induced spindle off-centering by codepleting MCAK. Supplementary time-lapse Deconvolution microscopy movies 1, 2 and 3 show spindle rotation or gliding movements in cells treated with Control or Control siRNA, respectively.

ACKNOWLEDGEMENTS

We thank the Pines group for the plasmid vector encoding Pericentrin fragment and the McAinsh and Straube groups for the He La cell line expressing Tomato-EB3. We thank Viviane Boilot and Nicholas Levin for support with image analysis. This work was supported by a Cancer Research UK Career Development Award (C28598/A9787) and QMUL Laboratory start-up grant to VMD, a Brunei Darussalam PhD studentship to IZ, a QMUL PhD studentship to MH, a LIDo BBSRC-DTP PhD studentship to DD (cosupervised by VMD and NS) and an Islamic Development Bank PhD studentship to PG.

The authors declare no competing financial interests.

Author contributions:

IZ, JC, MH and RS designed and performed experiments, analysed and interpreted data. PG, TK, IK and DD analysed data. NS and VMD co-supervised DD. VMD planned the study, discussed experimental design, analysis, interpreted data and wrote the manuscript. VMD and MH edited the manuscript.

FIGURE LEGENDS

Figure 1

Equatorial spindle centering is an early mitotic event that is dependent on MARK2, but not LGN or PAR3

(a) Upper row: Cartoons of mitotic spindle in either equatorially (i) or longitudinally (ii) off-centered (left) *versus* centered (right) positions. Spindles were scored as off-centered when the two distances (d_1 and d_2; marked by arrows) were unequal by greater than 20%. Lower row: Time-lapse images of Control siRNA transfected HeLa $^{His2B\text{-}GFP;mCherry\text{-}Tub}$ cells, acquired once every four minutes, showing normal equatorial spindle centering prior to longitudinal centering and oscillation along the pole-pole axis. Outline of cell cortex identified using cytoplasmic signal of mCherry-Tubulin is marked in yellow; pole-to-pole axis marked with yellow dashed line. Scale bar: 15μm (**b and c**) Temporal evolution of spindle centering along equatorial axis (b) and corresponding spindle maturation (from bent to straight bipolar spindle) (c) in seven representative cells from movies acquired as shown in (a). Boxes corresponding to sequential time frames in the movie are coloured either in red to indicate off-centered (b), or immature (c) spindles, or in green to indicate centered (b), or mature (c) spindles. (**d**) Experimental regime showing time-line of siRNA treatment followed by microscopy and lysate collection for immunoblotting to register protein depletion extent. (**e**) Time-lapse images of HeLa $^{His2B\text{-}GFP;mCherry\text{-}Tub}$ cells treated with control or LGN siRNA showing normal spindle centering, but no oscillation of the mitotic spindle or Par3-2 siRNA showing normal centering of the mitotic spindle or MARK2-1 siRNA showing equatorially off-centering of the mitotic spindle. Scale bar: 10μm. OC and C refer to equatorially off-centered and centered spindles, respectively. (**f-h**) Blot showing depletion extent of LGN (**f**), PAR3 (**g**) or MARK2 (**h**) using one or two different siRNA oligos. (**i-k**) Graph of percentage of equatorially centred spindles, at 8 or 12 min following NEBD, in Control or LGN siRNA treated cells (**i**), Control or PAR3-2 siRNA treated cells (**j**) and Control or MARK2-1 siRNA treated cells (**k**) as assessed from time-lapse movies of HeLa$^{His2B\text{-}GFP;mCherry\text{-}Tub}$ cells as shown in (e). Note that post-siRNA transfection time-matched control siRNA data are used for graphs and immunoblots. Error bars refer to SEM values from three independent experiments. P values showing significant (*) or insignificant (#) differences were calculated using Proportion test.

Figure 2

MARK2 is required for equatorial spindle centering up to anaphase

(**a**) Representative single plane deconvolved images of Z-stack movies of HeLa$^{His2B\text{-}GFP;\ mCherry\text{-}Tub}$ cells treated with MARK2 or Control siRNA oligos as indicated. Only cherry-Tubulin signals are shown for clarity. Scale bar: 5 μm. Yellow arrows point to off-centered spindles. Yellow circles highlight cell cortex. Note that the cell showed in MARK2-1 row is shown in Fig 1e. (**b**) Graph of percentage of mitotic cells with equatorially centered spindles at 8 minutes or 12 minutes following nuclear envelope breakdown (NEBD). (**c**) Uncropped immunoblot showing the expression of siRNA resistant MARK2-siRes-GFP in cells treated with control or MARK2 siRNA. Lysates of HeLa$^{MARK2\text{-}siRes\text{-}GFP}$ cells treated with siRNA and exposed to Tetracycline as indicated were immunoblotted with antibody against hMARK2; anti-gamma-tubulin antibody was used as loading control. Endogenous MARK2 and Tet-inducible siRNA resistant MARK fused with YFP are shown with arrows. (**d**) Bar graph showing the percentage of mitotic HeLa$^{MARK2\text{-}siRes\text{-}GFP}$ cells with equatorially centered spindles. Control or MARK2-1 siRNA treated HeLa$^{MARK2\text{-}siRes\text{-}GFP}$ cells in the presence or absence of Tetracycline (as indicated) were treated with MG132 to arrest them at metaphase prior during live-cell imaging. Cell expressing (green; +) or not-expressing (non-green, -) siRNA resistant form of MARK2-siRes-GFP were imaged and chromosome positions were ascertained using DIC, which was used to determine equatorially centered or off-centered metaphase plates. (**e**) Bar graph comparing the extent of equatorial centering of spindles at 8 minutes following NEBD *versus* anaphase onset in control or MARK2-1 siRNA treated cells, as assessed from time-lapse movies as shown in (**a**). Error bars represent SEM across 3 experimental repeats. p-values were obtained using Proportion test on percentage values. * and # indicates significant and insignificant difference respectively.

Figure 3

Off-centered spindles in MARK2-depleted cells fail to rotate properly towards the pre-determined spindle position at anaphase

(**a**) Representative time-lapse images of HeLa$^{His2B\text{-}GFP;mCherry\text{-}Tub}$ cells treated with siRNA as indicated. Final spindle (pole-to-pole) axis at anaphase onset (blue dashed

line) and interphase long-axis (yellow dashed line) are shown. Biased spindle rotation (green bar) and spindle orientation maintenance and oscillation (orange bar) regimes, off-centered spindle gliding proximal to the cortex (blue bar) are all indicated. OC and C refer to equatorially off-centered and centered spindles respectively. (**b**) Graph showing percentage of cells with centered or off-centered spindles that displayed no movements, gliding or oscillatory movements, as assessed from time-lapse movies of $HeLa^{His2B\text{-}GFP;mCherry\text{-}Tub}$ cells treated with control or MARK2-1 siRNA as indicated. (**c**) Distribution of final spindle orientation angles relative to interphase long-axis in cells as assessed from time-lapse movies of $HeLa^{His2B\text{-}GFP;mCherry\text{-}Tub}$ cells treated with control or MARK2-1 siRNA as in (a). p-value was obtained using Proportion test on percentage values. (**d**) Table summarizing (i) spindle position (equatorial centering success), (ii) spindle movement (oscillatory, rotational or gliding) and (iii) anaphase spindle orientation bias along interphase long-axis in MARK2 or control siRNA treated cells.

Figure 4

MARK2 regulates mitotic microtubule growth rate and function

(a) Single plane deconvolved images of cells immunostained with antibodies against anti-β-tubulin following control or MARK2-1 siRNA treatment. Scale bar: 5 μm. Gray scale image signals are inverted to highlight astral microtubule length and density. (**b)** Graph comparing the distribution of instantaneous velocities of EB3 comets in cells expressing EB3-mKate and treated with either MARK2 or control siRNA. Values were obtained manually by clicking spots using Softworx^{TM} Software. Non-overlapping peak values between control and MARK2 siRNA treated cells signify statistically significant differences (*) as confirmed by $p<0.01$ using the Proportion test. Error bars are SEM values across cells from two independent repeats. (**c**) Bar graph shows frequency distribution of spindle polarity (based on number of spindle poles: one (mono), two (bi), 3 to 4 or greater than 5). Cells were treated with siRNA as indicated, exposed to 1.7 μM Nocodazole for 3 hours to depolymerize all microtubules, recovered for 10 minutes in Nocodazole-free medium to reassemble spindles and immunostained using α-tubulin antibody. 100 nM 2ME2 was added in the recovery medium of Control siRNA treated cells. Error bars represent SEM from 3 independent experiments.

Figure 5

Cortical Dynein distributions but not spindle movement rates are perturbed following MARK2 depletion.

(**a**) Representative images of DHC-GFP signals in HeLa$^{DHC\text{-}GFP}$ cells, treated with the indicated siRNA, from time-lapse movies acquired once every minute. Cells were arrested at metaphase with MG132 treatment immediately prior to imaging. Spindle poles are marked with yellow and red asterisks to follow spindle movements. Blue and green arrowheads refer to 'crescent' or 'diffuse' DHC-GFP signals, respectively. Scale bar: 3 μm (**b**) Bar graph shows frequency distributions of DHC-GFP localisations in cell treated with the indicated siRNA oligos. Data collated over three independent experiments. (**c**) Graph shows frequency distribution of spindle pole displacement in HeLa cells treated with MG132 immediately prior to imaging. Values are obtained from time-lapse movies obtained in (a). 'n' refers to spindle positions acquired from at least 15 cells for each RNAi condition from 3 independent experiments. Distances are measured from the spindle pole furthest away from the cortex in the first frame, with the distance measured each subsequent frame for that specific pole. Error bars show SEM values.

Figure 6

Equatorial spindle off-centering following MARK2 depletion is not due to excessive pull by cortical Dynein.

(**a**) Representative time-lapse images of HeLa$^{His2B\text{-}GFP;mCherry\text{-}Tub}$ cells treated with siRNA as indicated. Equatorially centered (C) and off-centered (OC) spindles are marked. mCherry Tubulin signal is used to outline cell cortex (yellow circles) and pole-to-pole axis is marked using dashed yellow line. (**b**) Graph of percentage of equatorially centred spindles in cells treated with control or LGN with MARK2-1 siRNA, assessed from time-lapse movies as in (a). Spindle positions 8 mins after NEBD or at Anaphase are reported. (**c**) Temporal evolution of spindle positions in five representative cells, treated with siRNA as indicated, assessed from time-lapse movies as in (**a**). 'A' refers to anaphase. Red and green boxes indicate equatorially off-centered and centered spindle states, respectively. (**d**) Bar graph shows frequency distributions of DHC-GFP localisations in HeLa$^{DHC\text{-}GFP}$ cells treated with the

indicated siRNA oligos, as assessed from time-lapse movies acquired once every minute. Data collated over three independent experiments.

Figure 7

Aberrant equatorial centering and Dynein distribution following MARK2 depletion can be rescued by MCAK depletion

(**a**) Immunoblots show depletion extent of MARK2 and MCAK in lysates of HeLa$^{His2B\text{-}GFP;mCherry\text{-}Tub}$ cells following siRNA treatment with siRNA oligos as indicated. γ-tubulin is used as loading control. (**b**) Representative time-lapse images of HeLa$^{His2B\text{-}GFP;mCherry\text{-}Tub}$ cells treated with siRNA against MARK2 or MCAK alone or both MCAK and MARK2. Equatorially centered (C) and off-centered (OC) spindles are marked. mCherry Tubulin signal alone is shown and the signal was used to outline the cell cortex (yellow circles). (**c**) Graph of percentage of equatorially centered spindles, assessed from time-lapse movies as in (**b**). (**d**) Temporal evolution of spindle positions in five representative cells, treated with indicated siRNA, showing normal re-centering of equatorially off-centered spindles in cells treated with siRNA against either MCAK alone or both MCAK and MARK2 but not MARK2 alone. A refers to anaphase. Red and green boxes indicate equatorially off-centered and centered spindles, respectively. (**e**) Representative live-cell images of HeLa$^{DHC\text{-}GFP}$ cells treated with the indicated siRNA oligos. Yellow arrows mark cortical DHC-GFP localization. (**f**) Bar graph shows percentage of HeLa$^{DHC\text{-}GFP}$ cells with crescent or diffused cortical Dynein localization following treatments with the indicated siRNA oligos. Data collated over three independent experiments. (**g**) Successful spindle rotation requires equatorial centering: Cartoon shows two separate pathways governing equatorial and longitudinal spindle positions: (i) LGN directly controls cortical Dynein recruitment and in turn cortical Dynein mediated pull that powers spindle displacement (blue arrows). (ii) In contrast, MARK2/Par1b controls astral microtubule length and dynamics and ensures equatorial spindle centering (orange arrows). Both equatorial centering mediated by MARK2 and cortical pulling powered by Dynein are needed for successful spindle rotation. Equatorial off-centering and longitudinal oscillations have an indirect impact on cortical Dynein crescent formation (grey arrow).

SUPPLEMENTARY DATA

Supplementary Figure 1

MARK2 but not MARK3 is required for equatorial spindle centering

(**a**) Evolution of spindle positions relative to the geometrical center of the cell in seven representative cells from movies acquired as shown in figure 3b. Boxes corresponding to sequential time-frames of time-lapse movies are shown either as equatorially off centered (red), or centered (green) spindles. MARK2-1 and MARK2-2 siRNA oligo treated cells are compared against matched controls presented in Fig 2. (**b**) Images of mitotic HeLa$^{MARK2\text{-}siRes\text{-}GFP}$ cells showing metaphase plate position (DIC) and GFP expression following treatment with control or MARK2-1 siRNA. Cells expressing (green) or not-expressing (non-green) siRNA resistant form of MARK2-siRes-GFP were filmed in the presence of MG132. Position of metaphase plate used to infer equatorial spindle centering extent is marked with yellow asterisks. (**c**) Immunoblots showing depletion extent of MARK3 using two siRNA oligos against MARK3. Lysates collected following time-lapse imaging were immunostained using antibodies against MARK3; antibody against gamma-tubulin was used as loading control. (**d**) Graph of percentage of equatorially centered spindles in Control or MARK3 siRNA -treated HeLa$^{His2B\text{-}GFP;mCherry\text{-}Tub}$ cells, as assessed from time-lapse movies.

Supplementary Figure 2

Chromosome congression and segregation events are normal in cells depleted of MARK2

(**a**) Graph of percentage of HeLa$^{His2B\text{-}GFP;\ mCherry\text{-}Tub}$ cells treated with MARK2 or control siRNA oligos which underwent normal segregation of DNA into two sets, mitotic arrest (>90 mins), missegregation of DNA as lagging chromatids or underwent multipolar segregation. (**b-d**) Cumulative percentage graph of congression time (**b**), anaphase time (**c**) and congression to anaphase time (**d**) in cells treated with siRNAs as indicated. Congression time in minutes was measured as the time taken for the last chromosome to congress onto the metaphase plate starting from Nuclear Envelope Break Down (NEBD). NEBD, inferred from loss of nuclear intactness of His2B-GFP signals (in green) and nuclear exclusion of mcherry-Tubulin signals (in red), was marked as mitosis onset time = 0 min. Anaphase time in minutes was

measured as the time taken for the physical separation of DNA signal into two sets starting from NEBD. The difference between Congression and Anaphase times is shown in (d). (**e-g**) Bar graphs show average percentage values of mitotic cells that displayed normal mitotic cell rounding (**e**), spindle centering (**f**) or spindle orientation with the two poles on the same XY plane parallel to substratum (**g**). Values referring 8 and 12 minutes after NEBD or 8 and 4 minutes before anaphase onset are shown. n values refer to number of cells at least 4 independent repeats. Error bars refer to SEM values.

Supplementary Figure 3

MARK2 localises to centrosomes and cell cortex independent of microtubules in both interphase and mitosis

(**a-d**) Representative live-cell images of HeLa cells co-expressing exogenous MARK2-YFP and the centrosome localising PACT domain of pericentrin tagged with RFP to mark centrosomes. Images show the localisation of MARK2-YFP in unperturbed interphase (**a**) and metaphase (**b**) or after treatment with Nocodazole in interphase (**c**) and mitosis (**d**). Insets show magnified areas of centrosomes as indicated by white boxes on main images. Images of cells in mitosis are collected after a 60-minute treatment with MG132. For Nocodazole treatment, cells were exposed to 1.7 μM of Nocodazole for 30 minutes after MG132 treatment (Scale bars represent 10 μm in main image and 1 μm in insets).

Supplementary Figure 4

Co-depletion of MCAK rescues spindle off-centering and astral microtubule changes induced by MARK2 depletion

(a) Experimental regime showing time-line of siRNA treatment followed by ice-cold methanol treatment and immunostaining with anti-tubulin antibodies to image cold stable astral microtubules. **(b)** Representative deconvolved images of HeLa cells treated with siRNA and immunostained as indicated in (a). Images show longer astral microtubules in MARK2-depleted cells compared to Control-depleted cells or MARK2 and MCAK co-depleted cells. Scale bar: 10 μm. **(c-d)** Box plots showing cold stable astral microtubule lengths (c) and densities (d) following siRNA treatment, as indicated, in immunostained cells as shown in (b). Astral microtubule lengths are normalized using nearest distance between spindle pole and cell cortex to

exclude variation across off-centered and centered spindles. Horizontal line refers to median values, top and bottom of filled boxes refer to 75% and 25% values, respectively, and whiskers refer to min and max values. n values refer to number of cells from 3 independent experimental repeats. For density measurements, an area of 23 μm^2 was demarcated near the spindle pole area using the software Softworx^{TM}. **(e)** Representative deconvolved images of HeLa cells treated with siRNA and immunostained as indicated in (a) using antibodies against MCAK and EB3 **(f)** Bar graphs showing the average percentage of mitotic cells that display either equatorially centered spindles or mitotic cell rounding following siRNA treated as indicated using time-lapse movies as shown in Fig. 7b. n values refers to number of cells at least 3 independent repeats. Error bars refer to SEM values.

Supplementary Movies 1

Representative time-lapse Deconvolution microscopy movie of HeLa$^{His2B\text{-}GFP;\ mCherry\text{-}Tub}$ cells following Control siRNA treatment as indicated in Fig-2a. Pseudo-coloured in grey, green and red are DIC, GFP and mCherry, respectively. Representative movie shows normal equatorial centering, spindle rotation and spindle oscillation that are all initiated in prometaphase prior to the completion of chromosome congression. Frames were collected once every four minutes (frame display rate: 0.5s/frame).

Supplementary Movies 2

Representative time-lapse Deconvolution microscopy movie of HeLa$^{His2B\text{-}GFP;\ mCherry\text{-}Tub}$ cells following MARK2-1 siRNA treatment as indicated in Fig-2a. Pseudo-coloured in grey, green and red are DIC, GFP and mCherry, respectively. Representative movie shows equatorial off-centering in early mitosis that is rescued at metaphase- anaphase transition. Frames were collected once every four minutes (frame display rate: 0.5s/frame).

Supplementary Movies 3

Representative time-lapse Deconvolution microscopy movie of a HeLa$^{His2B\text{-}GFP;\ mCherry\text{-}Tub}$ cell treated with MARK2-1 and control siRNA treatment as indicated in Fig-7b. Pseudo-coloured in grey, green and red are DIC, GFP and mCherry, respectively. This movie is specifically chosen to highlight the gliding behavior of the spindle (and

lack of normal spindle rotation) in a MARK2-depleted cell with a prolonged prometaphase. Note the rescue of the off-centered spindle phenotype at metaphase-anaphase transition. Frames were collected once every four minutes (frame display rate: 0.5s/frame).

REFERENCES:

A force-generating machinery maintains the spindle at the cell center during mitosis. 2016. A force-generating machinery maintains the spindle at the cell center during mitosis. 352:1124–1127. doi:10.1126/science.aad9745.

A Semi-Supervised Approach for Refining Transcriptional Signatures of Drug Response and Repositioning Predictions. 2015. A Semi-Supervised Approach for Refining Transcriptional Signatures of Drug Response and Repositioning Predictions. 10:e0139446. doi:10.1371/journal.pone.0139446.

Andrews, P.D., Y. Ovechkina, N. Morrice, M. Wagenbach, K. Duncan, L. Wordeman, and J.R. Swedlow. 2004. Aurora B regulates MCAK at the mitotic centromere. *Dev. Cell*. 6:253–268.

Bessone, S., Vidal, F., Bouc, Y.L., Epelbaum, J., Bluet-Pajot, Darmon, M. 1999. EMK protein kinase-null mice: dwarfism and hypofertility associated with alterations in the somatotrope and prolactin pathways. 214:87–101. doi:10.1006/dbio.1999.9379.

Braun, A., K. Dang, F. Buslig, M.A. Baird, M.W. Davidson, C.M. Waterman, and K.A. Myers. 2014. Rac1 and Aurora A regulate MCAK to polarize microtubule growth in migrating endothelial cells. *The Journal of Cell Biology*. 206:97–112. doi:10.1083/jcb.201401063.

Carreno, S., I. Kouranti, E.S. Glusman, M.T. Fuller, A. Echard, and F. Payre. 2008. Moesin and its activating kinase Slik are required for cortical stability and microtubule organization in mitotic cells. *The Journal of Cell Biology*. 180:739–746. doi:10.1083/jcb.200709161.

Chin, H.M.S., K. Nandra, J. Clark, and V.M. Draviam. 2014. Need for multi-scale systems to identify spindle orientation regulators relevant to tissue disorganization in solid cancers. *Front Physiol*. 5:278. doi:10.3389/fphys.2014.00278.

Cohen, D., Brenwald, P., Rodriguez-Bouland and Musch, A. 2004. Mammalian PAR-1 determines epithelial lumen polarity by organizing the microtubule cytoskeleton. *The Journal of Cell Biology.* 164:717–727. doi:10.1083/jcb.200308104.

Collins, E.S., S.K. Balchand, J.L. Faraci, P. Wadsworth, and W.L. Lee. 2012. Cell cycle-regulated cortical dynein/dynactin promotes symmetric cell division by differential pole motion in anaphase. *Molecular Biology of the Cell*. 23:3380–3390. doi:10.1091/mbc.E12-02-0109.

Corrigan, A.M., R. Shrestha, V.M. Draviam, and A.M. Donald. 2015. Modeling of Noisy Spindle Dynamics Reveals Separable Contributions to Achieving Correct Orientation. *Biophys. J.* 109:1398–1409. doi:10.1016/j.bpj.2015.08.014.

Corrigan, A.M., R.L. Shrestha, I. Zulkipli, N. Hiroi, Y. Liu, N. Tamura, B. Yang, J. Patel, A. Funahashi, A. Donald, and V.M. Draviam. 2013. Automated tracking of mitotic spindle pole positions shows that LGN is required for spindle rotation but not orientation maintenance. *Cell Cycle*. 12:2643–2655. doi:10.4161/cc.25671.

Domnitz, S.B., M. Wagenbach, J. Decarreau, and L. Wordeman. 2012. MCAK activity at microtubule tips regulates spindle microtubule length to promote robust kinetochore attachment. *The Journal of Cell Biology*. doi:10.1083/jcb.201108147.

Draviam, V.M., I. Shapiro, B. Aldridge, and P.K. Sorger. 2006. Misorientation and reduced stretching of aligned sister kinetochores promote chromosome missegregation in EB1- or APC-depleted cells. *EMBO J*. 25:2814–2827. doi:10.1038/sj.emboj.7601168.

Drewes, G., Ebneth, A., Preuss, U., Mandelkow, E. M. and Mandelkow, E. 1997. MARK, a novel family of protein kinases that phosphorylate microtubule-associated proteins and trigger microtubule disruption. *Cell.* 89:297–308.

Drewes, G., Trinczek, B., Illenberger, S., Biernat, J., Schmitt-Ulms, G., Meyer, H.E., Mandelkow, E.M and Mandelkow, E. 1995. Microtubule-associated protein/microtubule affinity-regulating kinase (p110mark). A novel protein kinase that regulates tau-microtubule interactions and dynamic instability by phosphorylation at the Alzheimer-specific site serine 262. *J. Biol. Chem.* 270:7679–7688.

Dunsch, A.K., D. Hammond, J. Lloyd, L. Schermelleh, U. Gruneberg, and F.A. Barr. 2012. Dynein light chain 1 and a spindle-associated adaptor promote dynein asymmetry and spindle orientation. *The Journal of Cell Biology*. 198:1039–1054. doi:10.1083/jcb.201202112.

Guo, S., and K.J. Kemphues. 1995. par-1, a gene required for establishing polarity in C. elegans embryos, encodes a putative Ser/Thr kinase that is asymmetrically distributed. *Cell*. 81:611–620.

Hayashi, K., Suzuki, A., Hirai, S., Kurihara, Y., Hoogenraad, C. and Ohno S. 2011. Maintenance of dendritic spine morphology by partitioning-defective 1b through regulation of microtubule growth. *J. Neurosci.* 31:12094–12103. doi:10.1523/JNEUROSCI.0751-11.2011.

Hoopen, R. T., Cepeda-Gardia, C., Fernandez-Arruti, R., Juanes, M., Delgehyr, N. and Segal, M. 2012. Mechanism for astral microtubule capture by cortical Bud6p priming spindle polarity in *S. cerevisiae. Current Biology.* 22:1075–1083. doi:10.1016/j.cub.2012.04.059.

Huisman, S. M. and Segal, M. 2005. Cortical capture of microtubules and spindle polarity in budding yeast - where's the catch? *Journal of Cell Science.* 118:463–471. doi:10.1242/jcs.01650.

Hurov, J. and Piwnica-Worms. 2007. The Par-1/MARK family of protein kinases: from polarity to metabolism. *Cell Cycle.* 6:1966–1969.

Illenberger, S., Drewes, G., Trinczek, B., Biernat, J., Meyer, H.E., Olmsted, B. J., Mandelkow, E.M. and Mandelkow, E.M. 1996. Phosphorylation of microtubule-associated proteins MAP2 and MAP4 by the protein kinase p110mark. *J. Biol. Chem.* 271:10834–10843.

Kaji, N., A. Muramoto, and K. Mizuno. 2008. LIM kinase-mediated cofilin phosphorylation during mitosis is required for precise spindle positioning. *J Biol Chem*. 283:4983–4992. doi:10.1074/jbc.M708644200.

Kimura, K., and A. Kimura. 2011. A novel mechanism of microtubule length-dependent force to pull centrosomes toward the cell center. *BioArchitecture*. 1:74–79. doi:10.4161/bioa.1.2.15549.

Kiyomitsu, T., and I.M. Cheeseman. 2012. Chromosome- and spindle-pole-derived signals generate an intrinsic code for spindle position and orientation. *Nat. Cell Biol.* 14:311–317. doi:10.1038/ncb2440.

Kline-Smith, S.L., A. Khodjakov, P. Hergert, and C.E. Walczak. 2004. Depletion of Centromeric MCAK Leads to Chromosome Congression and Segregation Defects Due to Improper Kinetochore Attachments. *Molecular Biology of the Cell*. 15:1146. doi:10.1091/mbc.E03-08-0581.

Kotak, S., C. Busso, and P. Gonczy. 2012. Cortical dynein is critical for proper spindle positioning in human cells. *The Journal of Cell Biology*. 199:97–110. doi:10.1083/jcb.201203166.

Kunda, P., A.E. Pelling, T. Liu, and B. Baum. 2008. Moesin controls cortical rigidity, cell rounding, and spindle morphogenesis during mitosis. *Current biology : CB*. 18:91–101. doi:10.1016/j.cub.2007.12.051.

Kulukian, A. and E. Fuchs. 2013. Spindle orientation and epidermal morphogenesis. *Philosophical Transactions of The Royal Society*: 368: 20130016. doi:10.1098/rstb.2013.0016

Laan, L., N. Pavin, J. Husson, G. Romet-Lemonne, M. van Duijn, M.P. López, R.D. Vale, F. Jülicher, S.L. Reck-Peterson, and M. Dogterom. 2012. Cortical Dynein Controls Microtubule Dynamics to Generate Pulling Forces that Position Microtubule Asters. *Cell*. 148:502–514. doi:10.1016/j.cell.2012.01.007.

Macara, I.G., R. Guyer, G. Richardson, Y. Huo, and S.M. Ahmed. 2014. Epithelial homeostasis. *Current biology: CB*. 24:R815–25. doi:10.1016/j.cub.2014.06.068.

Mandelkow, E.M. 2004. MARK/PAR1 kinase is a regulator of microtubule-dependent transport in axons. *The Journal of Cell Biology*. 167:99–110. doi:10.1083/jcb.200401085.

Markus, S. and Lee, W. 2011. Regulated offloading of cytoplasmic dynein from microtubule plus ends to the cortex. *Developmental Cell* 20:639–651. doi:10.1016/j.devcel.2011.04.011.

Matsumura, S., M. Hamasaki, T. Yamamoto, M. Ebisuya, M. Sato, E. Nishida, and F. Toyoshima. 2012. ABL1 regulates spindle orientation in adherent cells and

mammalian skin. *Nat Commun*. 3:626. doi:10.1038/ncomms1634.

Mitsushima, M., F. Toyoshima, and E. Nishida. 2009. Dual role of Cdc42 in spindle orientation control of adherent cells. *Molecular and Cellular Biology*. 29:2816–2827. doi:10.1128/MCB.01713-08.

Nakai, Y., M. Ozeki, T. Hiraiwa, R. Tanimoto, A. Funahashi, N. Hiroi, A. Taniguchi, S. Nonaka, V. Boilot, R. Shrestha, J. Clark, N. Tamura, V.M. Draviam, and H. Oku. 2015. High-speed microscopy with an electrically tunable lens to image the dynamics of in vivo molecular complexes. *Rev Sci Instrum*. 86:013707. doi:10.1063/1.4905330.

Nishimura, Y., K. Applegate, M.W. Davidson, G. Danuser, and C.M. Waterman. 2012. Automated screening of microtubule growth dynamics identifies MARK2 as a regulator of leading edge microtubules downstream of Rac1 in migrating cells. *PLoS ONE*. 7:e41413. doi:10.1371/journal.pone.0041413.

O'Connell, C.B., and Y.L. Wang. 2000. Mammalian spindle orientation and position respond to changes in cell shape in a dynein-dependent fashion. *Molecular Biology of the Cell*. 11:1765–1774.

Patel, H., Stavrou, I., Shrestha, R., Draviam, V., Frame, M. and Brunton, V. 2016. Kindlin1 regulates microtubule function to ensure normal mitosis. J Mol Cell Biol. 8:338–348. doi:10.1093/jmcb/mjw009.

Poser, I., M. Sarov, J.R.A. Hutchins, J.-K. Hériché, Y. Toyoda, A. Pozniakovsky, D. Weigl, A. Nitzsche, B. Hegemann, A.W. Bird, L. Pelletier, R. Kittler, S. Hua, R. Naumann, M. Augsburg, M.M. Sykora, H. Hofemeister, Y. Zhang, K. Nasmyth, K.P. White, S. Dietzel, K. Mechtler, R. Durbin, A.F. Stewart, J.-M. Peters, F. Buchholz, and A.A. Hyman. 2008. BAC TransgeneOmics: a high-throughput method for exploration of protein function in mammals. *Nat Meth*. 5:409–415. doi:10.1038/nmeth.1199.

Rizk, R.S., K.P. Bohannon, L.A. Wetzel, J. Powers, S.L. Shaw, and C.E. Walczak. 2009. MCAK and paclitaxel have differential effects on spindle microtubule organization and dynamics. *Molecular Biology of the Cell*. 20:1639–1651. doi:10.1091/mbc.E08-09-0985.

Roubinet, C., B. Decelle, G. Chicanne, J.F. Dorn, B. Payrastre, F. Payre, and S. Carreno. 2011. Molecular networks linked by Moesin drive remodeling of the cell cortex during mitosis. *The Journal of Cell Biology*. 195:99–112. doi:10.1083/jcb.201106048.

Samora, C.P., B. Mogessie, L. Conway, J.L. Ross, A. Straube, and A.D. McAinsh. 2011. MAP4 and CLASP1 operate as a safety mechanism to maintain a stable spindle position in mitosis. *Nat. Cell Biol.* 13:1040–1050. doi:10.1038/ncb2297.

Sato, Y., Akitsu, M., Amano, Y., Yamashita, K., Ide, M., Shimada, K., Yamashita, A., Hirano, H., Arakawa, N., Maki, T., Hayashi, I., Ohno, S. and Suzuki, A. 2013. The novel PAR-1-binding protein MTCL1 has crucial roles in organizing microtubules in polarizing epithelial cells. *Journal of Cell Science.* 126:4671–

4683.

Sato Y., Hayashi, K., Amano, Y., Takahashi, M., Yonemura, S., Hayashi, I., Hiorse, H., Ohno, S., Suzuki, A. 2014. MTCL1 crosslinks and stabilizes non-centrosomal microtubules on the Golgi membrane. *Nature Communications* 5:1–14. doi:10.1038/ncomms6266.

Schaar, B. T., Kinoshita, K. and McConnell, S. K. 2004. Doublecortin microtubule affinity is regulated by a balance of kinase and phosphatase activity at the leading edge of migrating neurons. *Neuron.* 41:203–213.

Sheeman, B., Carvalho, P., Sagot, I., Geiser, J., Kho, D., Hoyt, A. and Pellman, D. 2003. Determinants of S. cerevisiae dynein localization and activation: implications for the mechanism of spindle positioning. *Current Biology.* 13:364–372.

Shrestha, R.L., N. Tamura, A. Fries, N. Levin, J. Clark, and V.M. Draviam. 2014. TAO1 kinase maintains chromosomal stability by facilitating proper congression of chromosomes. *Open Biology*. 4. doi:10.1098/rsob.130108.

Shulman, J.M., Benton, R. and Johnston, D. 2000. The Drosophila homolog of C. elegans PAR-1 organizes the oocyte cytoskeleton and directs oskar mRNA localization to the posterior pole. *Cell* 101:377–388.

Slim, C.L., F. Lázaro-Diéguez, M. Bijlard, M.J.M. Toussaint, A. de Bruin, Q. Du, A. Müsch, and S.C.D. van Ijzendoorn. 2013. Par1b induces asymmetric inheritance of plasma membrane domains via LGN-dependent mitotic spindle orientation in proliferating hepatocytes. *PLoS Biol.* 11:e1001739. doi:10.1371/journal.pbio.1001739.

Syred, H.M., J. Welburn, J. Rappsilber, and H. Ohkura. 2013. Cell cycle regulation of microtubule interactomes: multi-layered regulation is critical for the interphase/mitosis transition. *Mol. Cell Proteomics*. 12:3135–3147. doi:10.1074/mcp.M113.028563.

Talapatra, S., Harker, B. and Welburn, J. The C-terminal region of the motor protein MCAK controls its structure and activity through a conformational switch. *eLife* 1–21. doi:10.7554/eLife.06421.001.

Tame, M.A., J.A. Raaijmakers, B. van den Broek, A. Lindqvist, K. Jalink, and R.H. Medema. 2014. Astral microtubules control redistribution of dynein at the cell cortex to facilitate spindle positioning. *Cell Cycle*. 13:1162–1170. doi:10.4161/cc.28031.

Tamura, N., and V.M. Draviam. 2012. Microtubule plus-ends within a mitotic cell are “moving platforms” with anchoring, signalling and force-coupling roles. *Open Biology*. 2:120132. doi:10.1098/rsob.120132.

Tamura, N., J.E. Simon, A. Nayak, R. Shenoy, N. Hiroi, V. Boilot, A. Funahashi, and V.M. Draviam. 2015. A proteomic study of mitotic phase-specific interactors of EB1 reveals a role for SXIP-mediated protein interactions in anaphase onset. *Biology Open*. doi:10.1242/bio.201410413.

Tergaonkar, V., D.V. Mythily, and S. Krishna. 1997. Cytokeratin patterns of expression in human epithelial cell lines correlate with transcriptional activity of the human papillomavirus type 16 upstream regulatory region. *J. Gen. Virol.* 78 (Pt 10):2601–2606. doi:10.1099/0022-1317-78-10-2601.

Toyoshima, F., and E. Nishida. 2007. Integrin-mediated adhesion orients the spindle parallel to the substratum in an EB1- and myosin X-dependent manner. *EMBO J.* 26:1487–1498. doi:10.1038/sj.emboj.7601599.

Toyoshima, F., S. Matsumura, H. Morimoto, M. Mitsushima, and E. Nishida. 2007. PtdIns(3,4,5)P3 regulates spindle orientation in adherent cells. *Dev. Cell*. 13:796–811. doi:10.1016/j.devcel.2007.10.014.

Tulu, U.S., C. Fagerstrom, N.P. Ferenz, and P. Wadsworth. 2006. Molecular requirements for kinetochore-associated microtubule formation in mammalian cells. *Current biology : CB*. 16:536–541. doi:10.1016/j.cub.2006.01.060.

Wühr, M., E.S. Tan, S.K. Parker, H.W. Detrich III, and T.J. Mitchison. 2010. A Model for Cleavage Plane Determination in Early Amphibian and Fish Embryos. *Current Biology*. 20:2040–2045. doi:10.1016/j.cub.2010.10.024.

Zhao, T., O.S. Graham, A. Raposo, and D. St Johnston. 2012. Growing microtubules push the oocyte nucleus to polarize the Drosophila dorsal-ventral axis. *Science*. 336:999–1003. doi:10.1126/science.1219147.

Zhu, J., A. Burakov, V. Rodionov, and A. Mogilner. 2010. Finding the cell center by a balance of dynein and myosin pulling and microtubule pushing: a computational study. *Molecular Biology of the Cell*. 21:4418–4427. doi:10.1091/mbc.E10-07-0627.

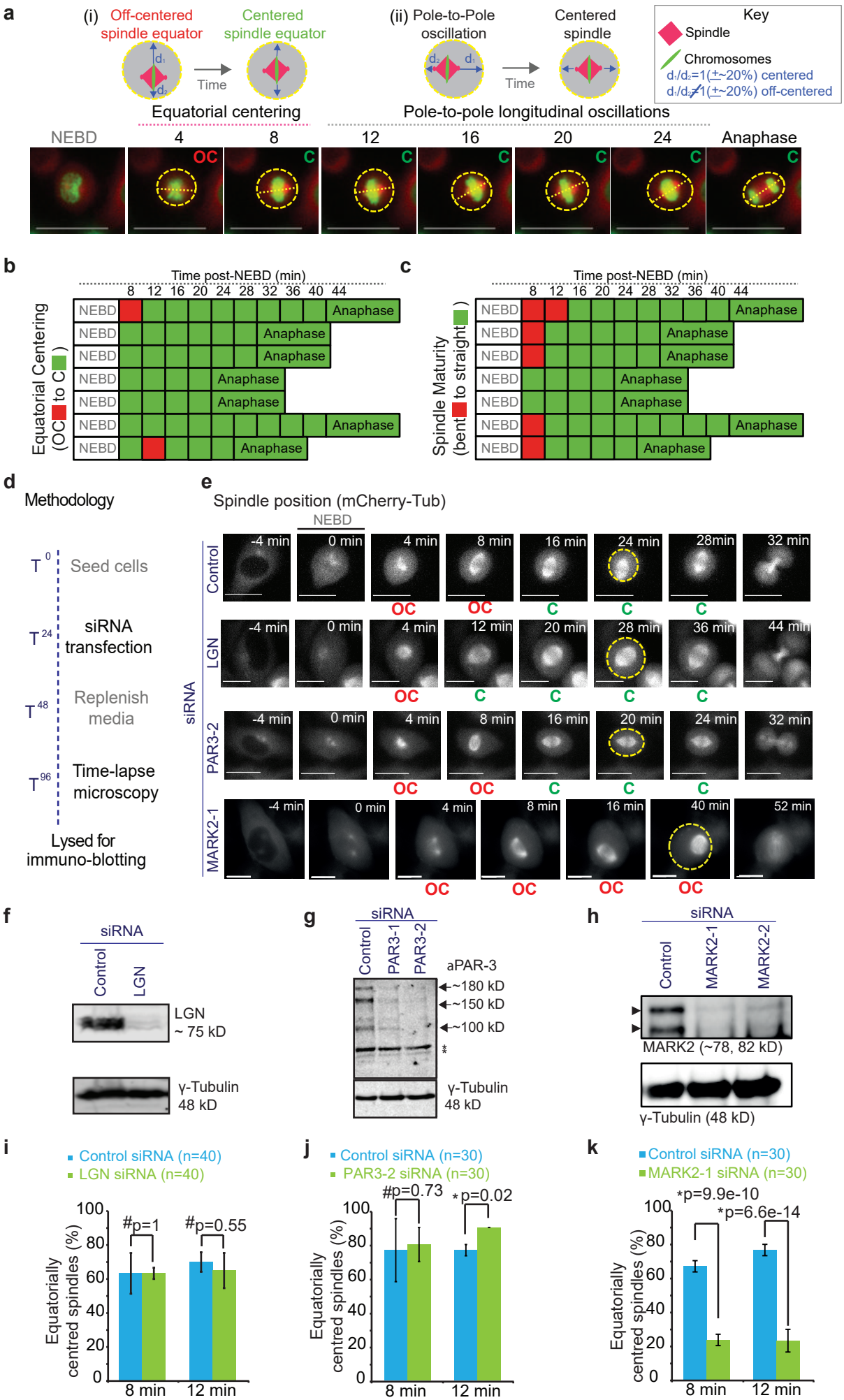
a
(i) Off-centered spindle equator
Centered spindle equator
Time
(ii) Pole-to-Pole oscillation
Centered spindle
Time
Key
Spindle
Chromosomes
d1/d2=1(±~20%) centered
d1/d2≠1(±~20%) off-centered
Equatorial centering
Pole-to-pole longitudinal oscillations
NEBD 4 8 12 16 20 24 Anaphase
OC
C
b
Time post-NEBD (min)
8 12 16 20 24 28 32 36 40 44
Equatorial Centering (OC to C)
NEBD
Anaphase
c
Time post-NEBD (min)
Spindle Maturity (bent to straight)
d
Methodology
T0 Seed cells
T24 siRNA transfection
T48 Replenish media
T96 Time-lapse microscopy
Lysed for immuno-blotting
e
Spindle position (mCherry-Tub)
NEBD
siRNA
Control
LGN
PAR3-2
MARK2-1
-4 min
0 min
4 min
8 min
12 min
16 min
20 min
24 min
28 min
28min
32 min
36 min
40 min
44 min
52 min
OC
C
f
siRNA
Control
LGN
LGN ~ 75 kD
γ-Tubulin 48 kD
g
siRNA
Control
PAR3-1
PAR3-2
aPAR-3
~180 kD
~150 kD
~100 kD
γ-Tubulin 48 kD
h
siRNA
Control
MARK2-1
MARK2-2
MARK2 (~78, 82 kD)
γ-Tubulin (48 kD)
i
Control siRNA (n=40)
LGN siRNA (n=40)
#p=1
#p=0.55
Equatorially centred spindles (%)
8 min
12 min
Time after NEBD
j
Control siRNA (n=30)
PAR3-2 siRNA (n=30)
#p=0.73
*p=0.02
k
Control siRNA (n=30)
MARK2-1 siRNA (n=30)
*p=9.9e-10
*p=6.6e-14

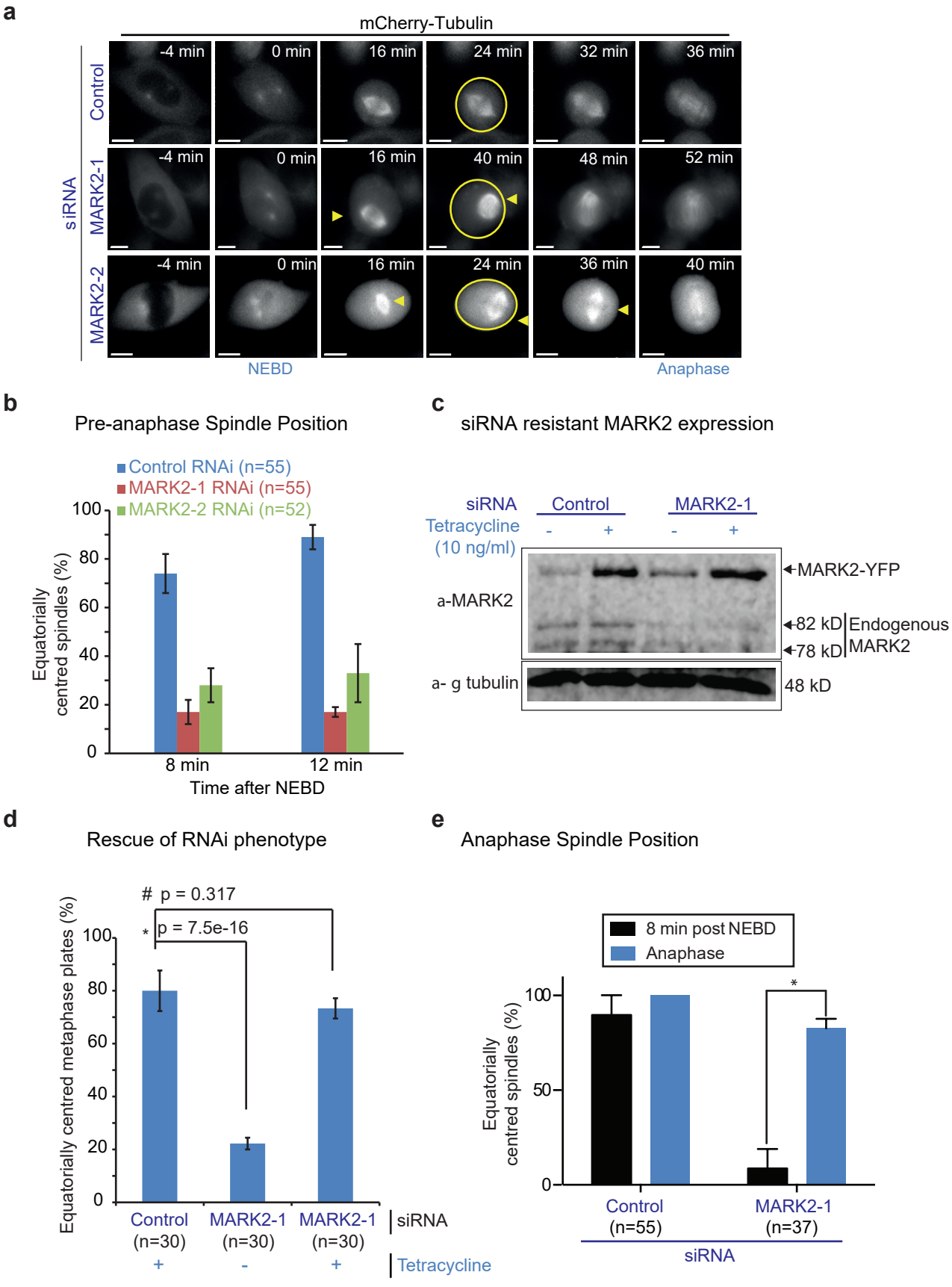
a
mCherry-Tubulin
siRNA
Control
MARK2-1
MARK2-2
-4 min
0 min
16 min
24 min
32 min
36 min
40 min
48 min
52 min
NEBD
Anaphase
b
Pre-anaphase Spindle Position
Control RNAi (n=55)
MARK2-1 RNAi (n=55)
MARK2-2 RNAi (n=52)
Equatorially centred spindles (%)
Time after NEBD
8 min
12 min
c
siRNA resistant MARK2 expression
siRNA
Control
MARK2-1
Tetracycline (10 ng/ml)
a-MARK2
MARK2-YFP
82 kD
78 kD
Endogenous MARK2
a- g tubulin
48 kD
d
Rescue of RNAi phenotype
p = 0.317
* p = 7.5e-16
Equatorially centred metaphase plates (%)
Control (n=30)
MARK2-1 (n=30)
MARK2-1 (n=30)
siRNA
Tetracycline
e
Anaphase Spindle Position
8 min post NEBD
Anaphase
Equatorially centred spindles (%)
Control (n=55)
MARK2-1 (n=37)
siRNA

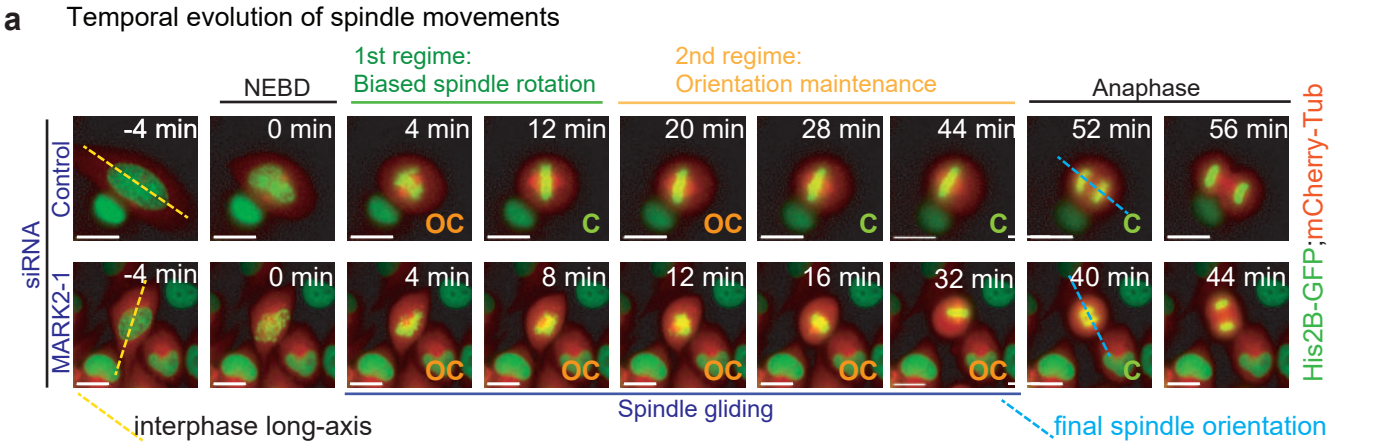

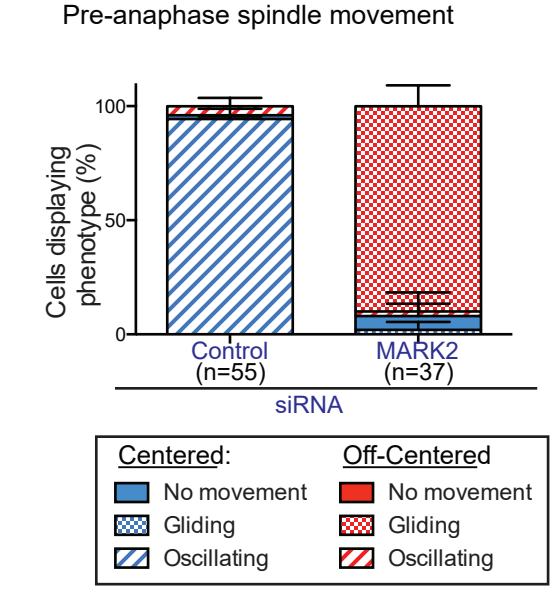

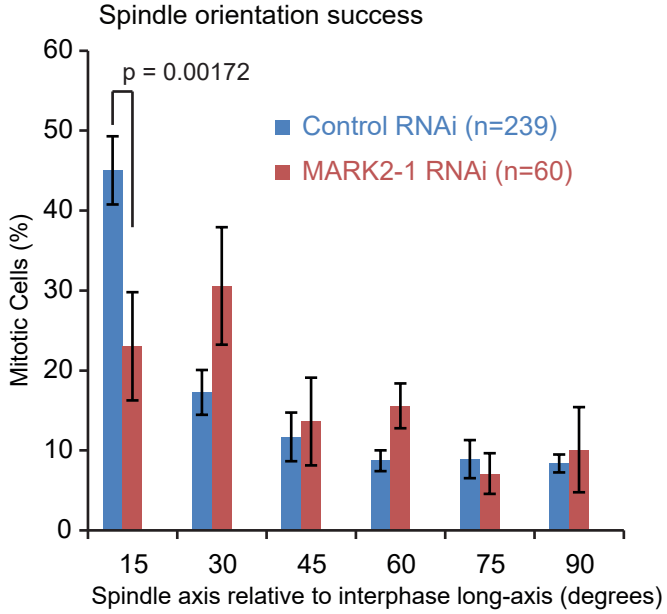

d

siRNA treatment	Equatorial spindle-centering			Spindle fate	
	8 min post NEBD	Metaphase	Anaphase	Movement	Orientation
Control	Centered	Centered	Centered	Rotation & Oscillation	Biased
MARK2	Off-centered	Off-centered	Centered	Gliding	Unbiased

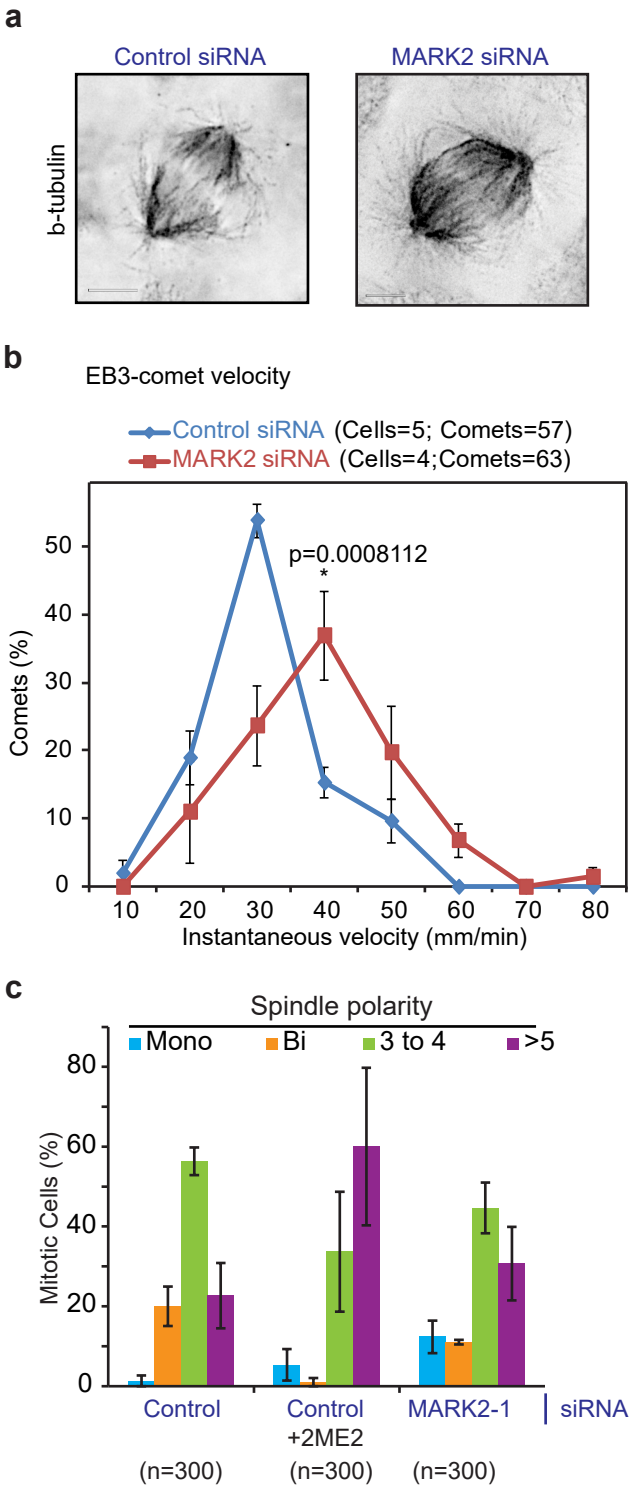
a
Control siRNA
MARK2 siRNA
b-tubulin
b
EB3-comet velocity
Control siRNA (Cells=5; Comets=57)
MARK2 siRNA (Cells=4;Comets=63)
p=0.0008112
*
Comets (%)
0
10
20
30
40
50
10
20
30
40
50
60
70
80
Instantaneous velocity (mm/min)
c
Spindle polarity
Mono
Bi
3 to 4
>5
Mitotic Cells (%)
0
20
40
60
80
Control
Control
+2ME2
MARK2-1
siRNA
(n=300)
(n=300)
(n=300)

a Spindle Position and Cortical Dynein Localisation

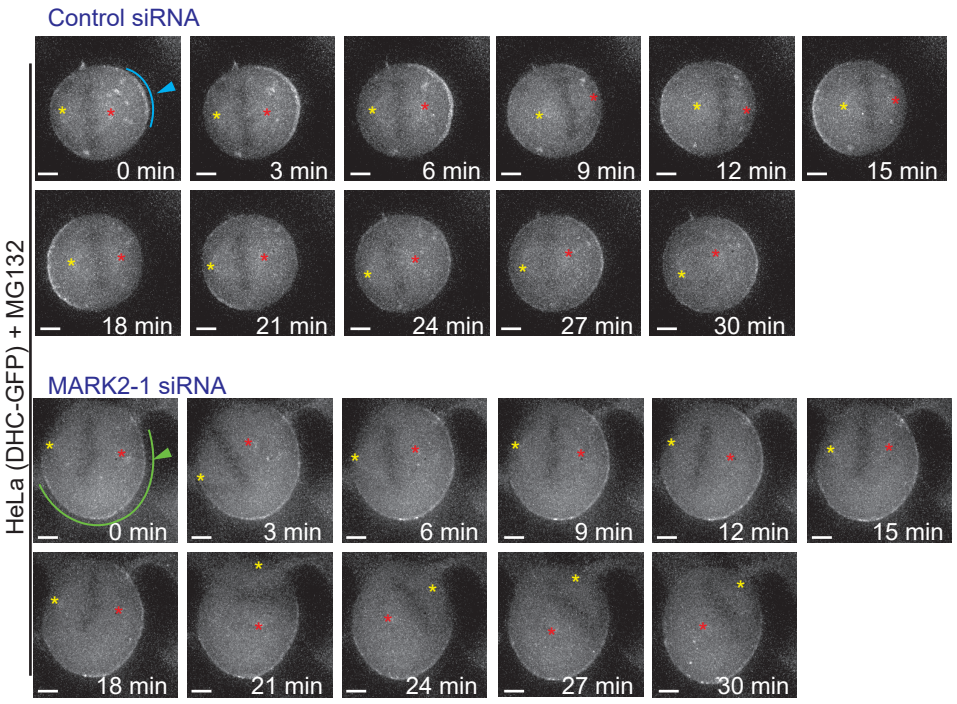

b Cortical Dynein Distributions

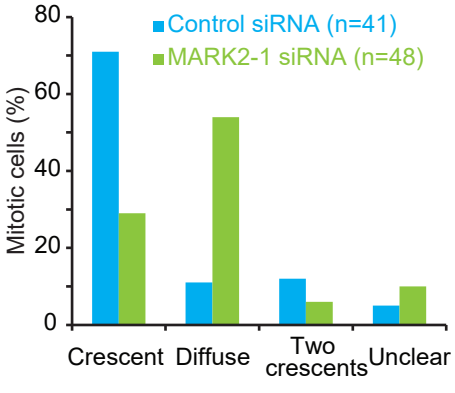

c Spindle movement rate

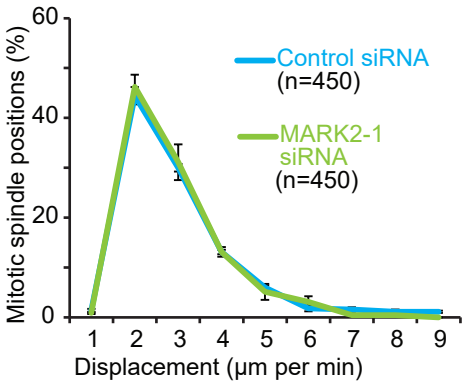

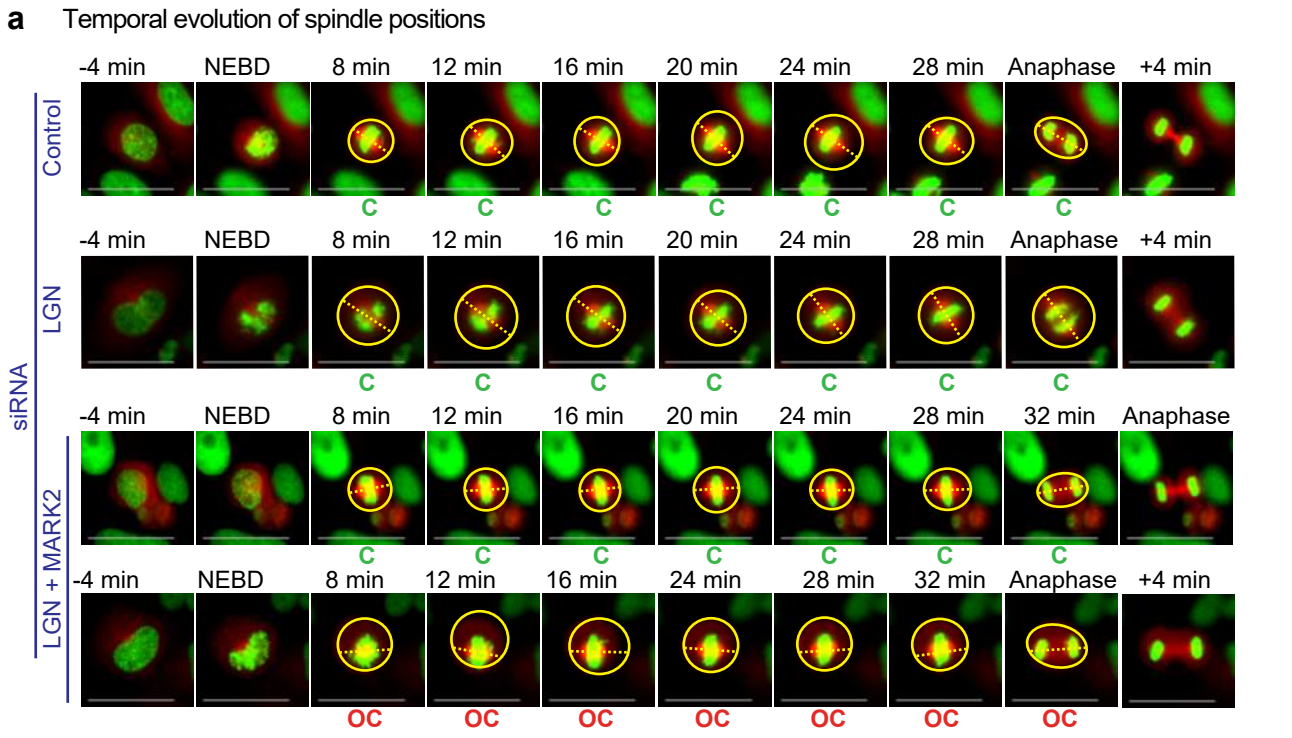
a
Temporal evolution of spindle positions
siRNA
Control
LGN
LGN + MARK2
-4 min
NEBD
8 min
12 min
16 min
20 min
24 min
28 min
32 min
Anaphase
+4 min
C
OC

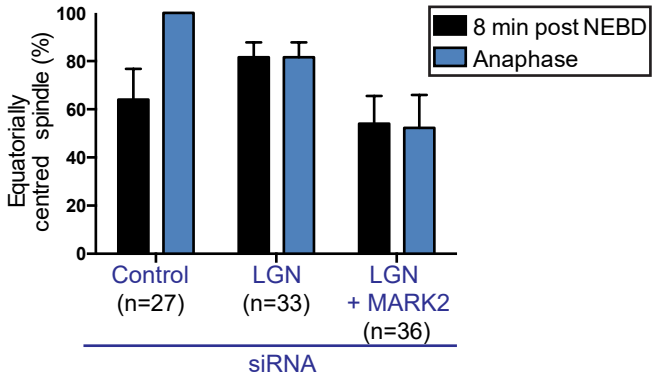
b
Spindle position
Equatorially centred spindle (%)
8 min post NEBD
Anaphase
Control (n=27)
LGN (n=33)
LGN + MARK2 (n=36)
siRNA

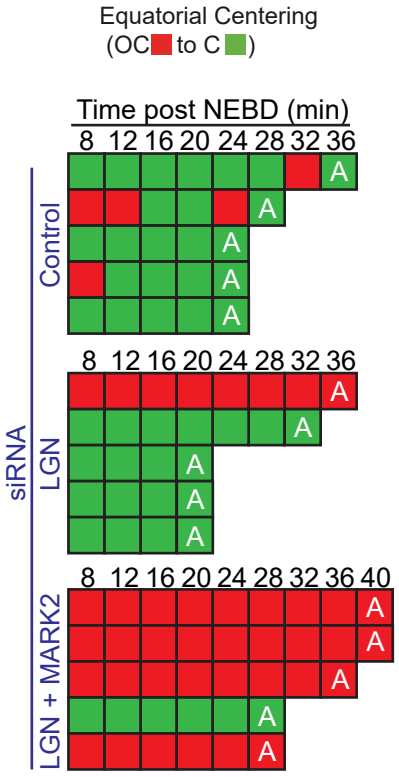
c
Equatorial Centering
(OC to C)
Time post NEBD (min)
Control
LGN
LGN + MARK2
siRNA
A

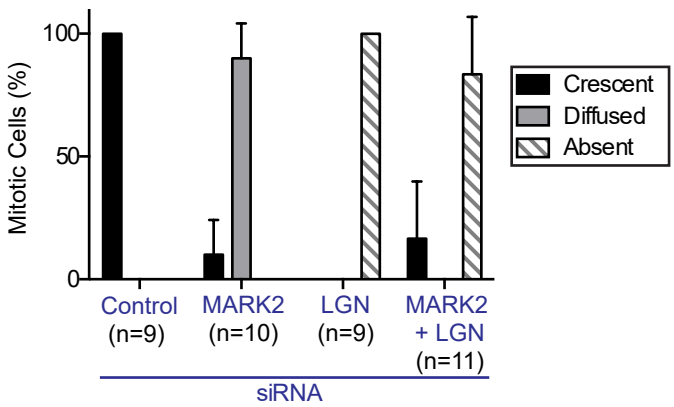
d
Cortical Dynein Distributions
Mitotic Cells (%)
Crescent
Diffused
Absent
Control (n=9)
MARK2 (n=10)
LGN (n=9)
MARK2 + LGN (n=11)
siRNA

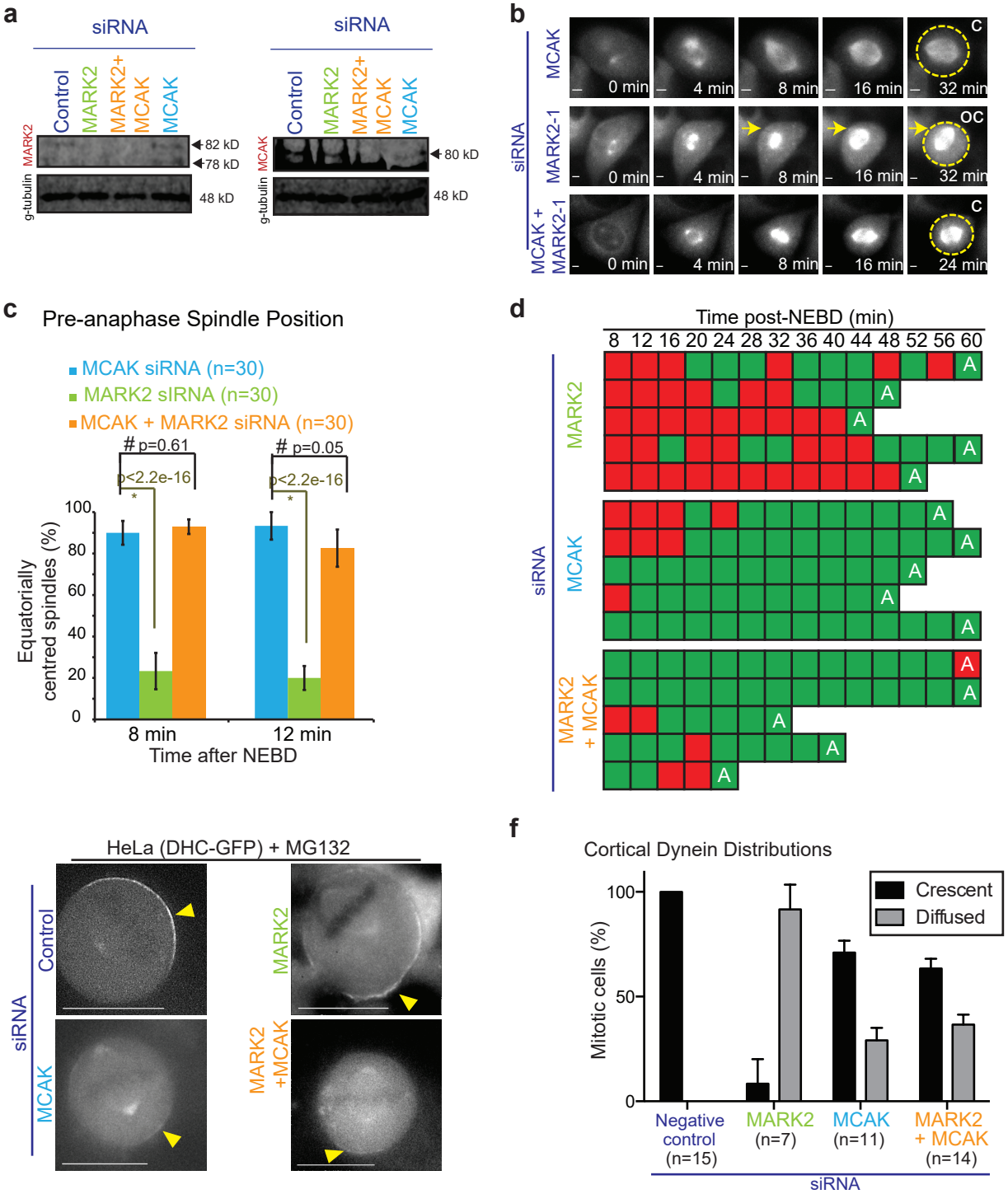
a
siRNA
Control
MARK2
MARK2+ MCAK
MCAK
82 kD
78 kD
MARK2
48 kD
g-tubulin
80 kD
MCAK
b
MCAK
MARK2-1
MCAK + MARK2-1
0 min
4 min
8 min
16 min
32 min
24 min
C
OC
c
Pre-anaphase Spindle Position
MCAK siRNA (n=30)
MARK2 sIRNA (n=30)
MCAK + MARK2 siRNA (n=30)
p=0.61
p<2.2e-16
p=0.05
p<2.2e-16
Equatorially centred spindles (%)
8 min
12 min
Time after NEBD
d
Time post-NEBD (min)
8 12 16 20 24 28 32 36 40 44 48 52 56 60
MARK2
MCAK
MARK2 + MCAK
A
e
HeLa (DHC-GFP) + MG132
Control
MARK2
MCAK
MARK2 +MCAK
f
Cortical Dynein Distributions
Crescent
Diffused
Mitotic cells (%)
Negative control (n=15)
MARK2 (n=7)
MCAK (n=11)
MARK2 + MCAK (n=14)
siRNA
g
Sucessful spindle rotation requires equatorial centering
LGN pathway
MARK2 pathway
Cortical Dynein recruitment
Cortical Dynein crescents
Cortical Dynein mediated pull
Reduce astral microtubule growth & length
(1) Pole-to-cortex oscillatory movements
(2) Equatorial centering movements

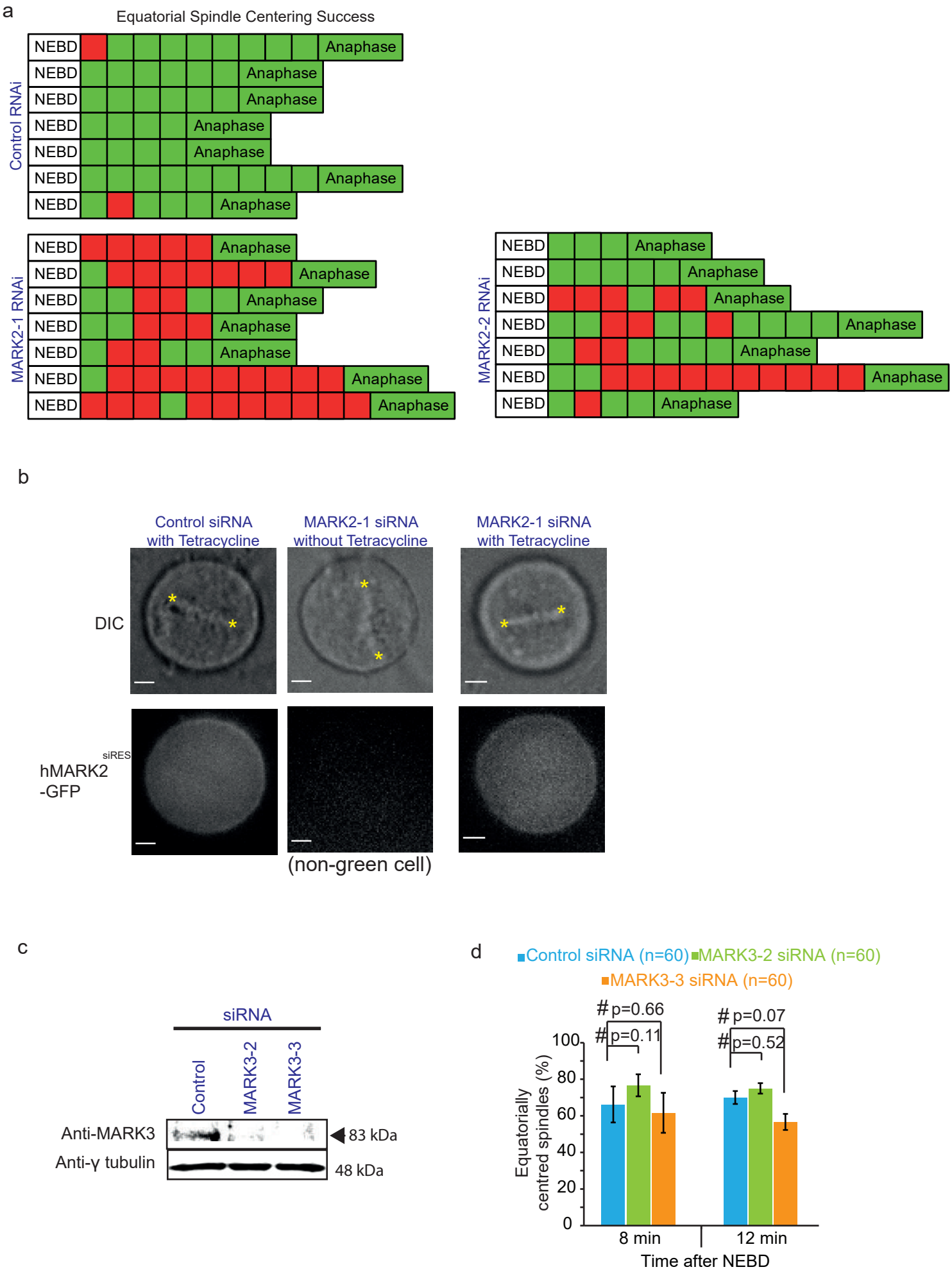
a
Equatorial Spindle Centering Success
Control RNAi
MARK2-1 RNAi
MARK2-2 RNAi
NEBD
Anaphase
b
Control siRNA with Tetracycline
MARK2-1 siRNA without Tetracycline
MARK2-1 siRNA with Tetracycline
DIC
siRES
hMARK2 -GFP
(non-green cell)
c
siRNA
Control
MARK3-2
MARK3-3
Anti-MARK3
Anti-γ tubulin
83 kDa
48 kDa
d
Control siRNA (n=60)
MARK3-2 siRNA (n=60)
MARK3-3 siRNA (n=60)
p=0.66
p=0.11
p=0.07
p=0.52
Equatorially centred spindles (%)
100
80
60
40
20
0
8 min
12 min
Time after NEBD

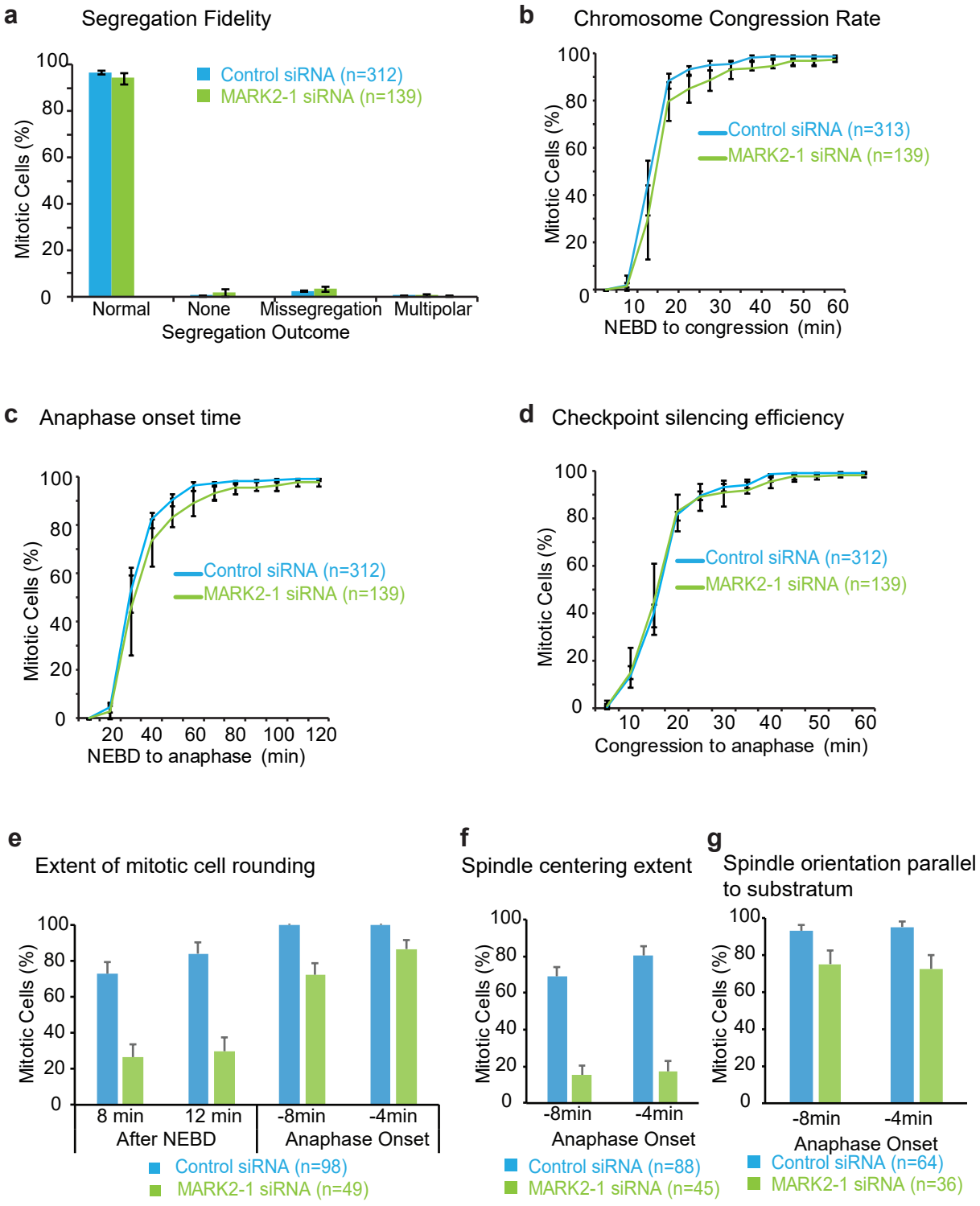
a
Segregation Fidelity
Mitotic Cells (%)
Control siRNA (n=312)
MARK2-1 siRNA (n=139)
Normal
None
Missegregation
Multipolar
Segregation Outcome
b
Chromosome Congression Rate
Mitotic Cells (%)
Control siRNA (n=313)
MARK2-1 siRNA (n=139)
NEBD to congression (min)
c
Anaphase onset time
Mitotic Cells (%)
Control siRNA (n=312)
MARK2-1 siRNA (n=139)
NEBD to anaphase (min)
d
Checkpoint silencing efficiency
Mitotic Cells (%)
Control siRNA (n=312)
MARK2-1 siRNA (n=139)
Congression to anaphase (min)
e
Extent of mitotic cell rounding
Mitotic Cells (%)
8 min
12 min
-8min
-4min
After NEBD
Anaphase Onset
Control siRNA (n=98)
MARK2-1 siRNA (n=49)
f
Spindle centering extent
Mitotic Cells (%)
-8min
-4min
Anaphase Onset
Control siRNA (n=88)
MARK2-1 siRNA (n=45)
g
Spindle orientation parallel to substratum
Mitotic Cells (%)
-8min
-4min
Anaphase Onset
Control siRNA (n=64)
MARK2-1 siRNA (n=36)

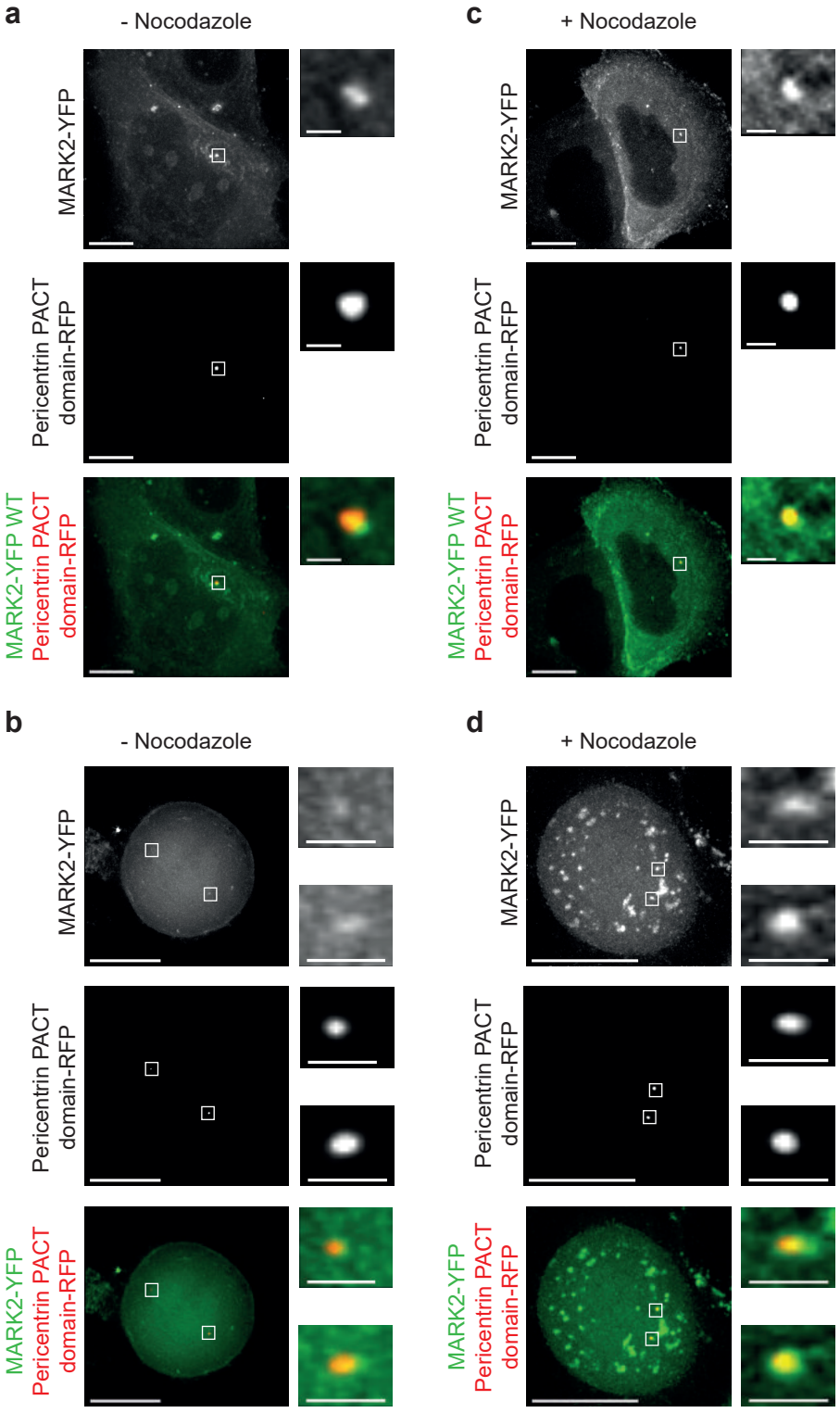
a
- Nocodazole
MARK2-YFP
Pericentrin PACT domain-RFP
MARK2-YFP WT Pericentrin PACT domain-RFP
c
+ Nocodazole
MARK2-YFP
Pericentrin PACT domain-RFP
MARK2-YFP WT Pericentrin PACT domain-RFP
b
- Nocodazole
MARK2-YFP
Pericentrin PACT domain-RFP
MARK2-YFP Pericentrin PACT domain-RFP
d
+ Nocodazole
MARK2-YFP
Pericentrin PACT domain-RFP
MARK2-YFP Pericentrin PACT domain-RFP

a

Cold stable astral MT studies

T^{0h} Seed cells

T^{24h} siRNA Transfection

T^{96h} 60 sec Ice-cold methanol fixation

Immunostaining

b

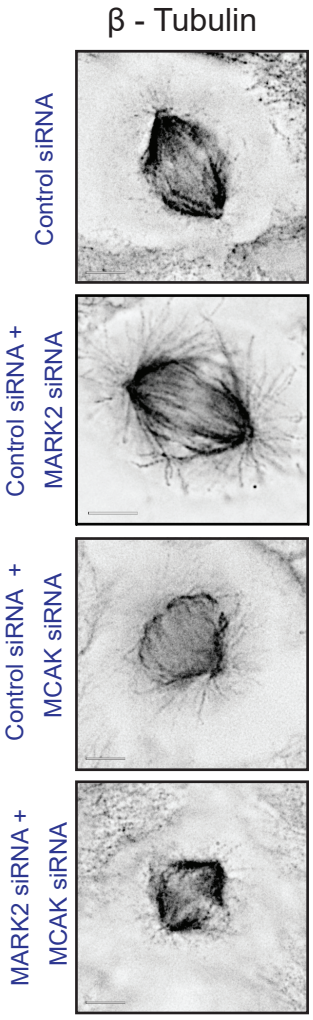

c

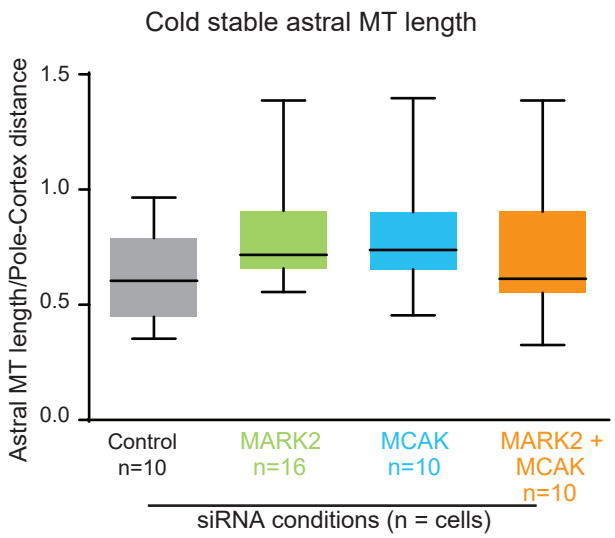

d

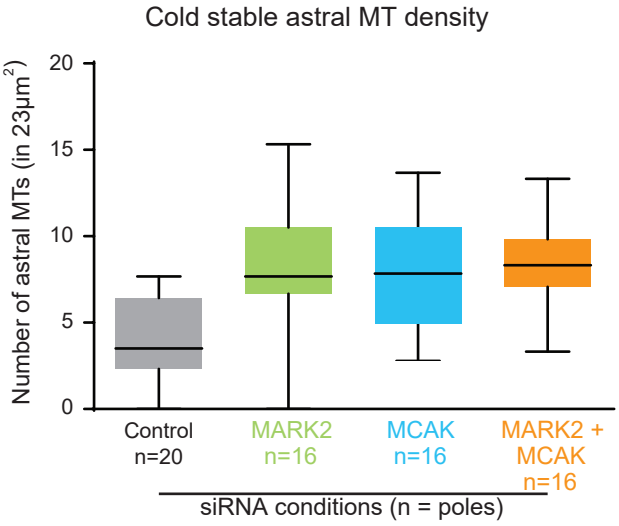

e

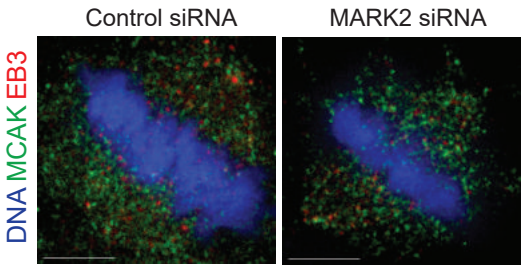

f